Backbone curve tailoring via Lyapunov subcenter manifold optimization

Pozzi, Matteo; Marconi, Jacopo; Jain, Shobhit; Braghin, Francesco

DOI
10.1007/s11071-024-09881-5

Publication date
2024

Document Version
Final published version

Published in
Nonlinear Dynamics

Citation (APA)
Pozzi, M., Marconi, J., Jain, S., & Braghin, F. (2024). Backbone curve tailoring via Lyapunov subcenter manifold optimization. *Nonlinear Dynamics*, *112*(18), 15719-15739. https://doi.org/10.1007/s11071-024-09881-5

Nonlinear Dyn
https://doi.org/10.1007/s11071-024-09881-5

RESEARCH

Backbone curve tailoring via Lyapunov subcenter manifold optimization

Matteo Pozzi · Jacopo Marconi · Shobhit Jain · Francesco Braghin

Received: 14 February 2024 / Accepted: 12 June 2024

Abstract We present a technique for the direct optimization of conservative backbone curves in nonlinear mechanical systems. The periodic orbits on the conservative backbone are computed analytically using the reduced dynamics of the corresponding Lyapunov subcenter manifold (LSM). In this manner, we avoid expensive full-system simulations and numerical continuation to approximate the nonlinear response. Our method aims at tailoring the shape of the backbone curve using a gradient-based optimization with respect to the system's parameters. To this end, we formulate the optimization problem by imposing constraints on the frequency-amplitude relation. Sensitivities are computed analytically by differentiating the backbone expression and the corresponding LSM. At each iteration, only the reduced-order model construction and sensitivity computation are performed, making our approach robust and efficient.

Keywords Parametric optimization · Backbone · Lyapunov subcenter manifold · Normal form · Reduced order modeling · Sensitivities

M. Pozzi · J. Marconi (✉) · F. Braghin
Department of Mechanical Engineering, Politecnico di Milano, Via G. La Masa, 1, 20156 Milan, MI, Italy
e-mail: jacopo.marconi@polimi.it

S. Jain
Delft Institute of Applied Mathematics, TU Delft, Mekelweg 4, 2628CD, ZH Delft, The Netherlands

Published online: 29 June 2024

List of symbols

$\boldsymbol{x} \in \mathbb{R}^n$	Displacement vector
$\boldsymbol{M} \in \mathbb{R}^{n\times n}$	Mass matrix
$\boldsymbol{K} \in \mathbb{R}^{n\times n}$	Stiffness matrix
$\boldsymbol{f}(\boldsymbol{x}) \in \mathbb{R}^n$	Nonlinear force vector
$\omega \in \mathbb{R}$	Eigenfrequency
$\boldsymbol{\phi} \in \mathbb{R}^n$	Mode shape vector
$\boldsymbol{z} \in \mathbb{R}^N$	State vector
$\boldsymbol{A} \in \mathbb{R}^{N\times N}$	State matrix
$\boldsymbol{B} \in \mathbb{R}^{N\times N}$	State mass matrix
$\boldsymbol{F}(\boldsymbol{z}) \in \mathbb{R}^N$	State nonlinear force vector
$\lambda \in \mathbb{C}$	Eigenvalue
$\boldsymbol{v} \in \mathbb{C}^N$	Right eigenvector
$\boldsymbol{u} \in \mathbb{C}^N$	Left eigenvector
$\tau \in \mathbb{C}$	Eigenvector normalization coefficient
$\mathcal{L}_i \in \mathbb{C}^{N\cdot 2^i \times N\cdot 2^i}$	Order-i cohomological operator
$\boldsymbol{h}_i \in \mathbb{C}^{N\cdot 2^i}$	Order-i cohomological vector
$\boldsymbol{W}_i \in \mathbb{C}^{N\times 2^i}$	Order-i Lyapunov subcenter manifold parametrization matrix
$\boldsymbol{R}_i \in \mathbb{C}^{2\times 2^i}$	Order-i reduced dynamics parametrization matrix
$\boldsymbol{p} \in \mathbb{C}^2$	Reduced dynamics coordinates
$\tilde{\boldsymbol{p}} \in \mathbb{C}^2$	Normalized version of $\boldsymbol{p}$
$\rho \in \mathbb{R}$	Magnitude of $\boldsymbol{p}$ in polar coordinates
$\theta \in \mathbb{R}$	Phase of $\boldsymbol{p}$ in polar coordinates
$\gamma_i \in \mathbb{R}$	Order-i backbone coefficient
$\boldsymbol{a} \in \mathbb{N}^N$	Extraction vector
$z \in \mathbb{R}$	Target component of $\boldsymbol{z}$

$Z \in \mathbb{R}$	Root mean squared amplitude of z
$J \in \mathbb{R}$	Objective function
$\boldsymbol{\mu} \in \mathbb{R}^m$	Design variables
$\boldsymbol{\mu}_L \in \mathbb{R}^m$	Design variables lower bound
$\boldsymbol{\mu}_U \in \mathbb{R}^m$	Design variables upper bound
$\Omega^\star \in \mathbb{R}$	Target frequency
$Z^\star \in \mathbb{R}$	Target root mean squared amplitude

1 Introduction

The importance of considering nonlinear effects in the design phase of a system has been by now widely demonstrated by an ever-increasing number of devices, in which nonlinearities are not merely a side effect to be avoided, but play their own functional role. Examples of this can be found in micro-mechanical resonators [1,2], micro-mass sensors [3,4], and micro-gyroscopes [5–7]. Other applications include frequency division [8], frequency stabilization [9,10], vibration energy harvesting [11,12], vibration mitigation [13–15], nonlinear energy sinks [16], and targeted energy transfer [17]. Usually, the frequency-amplitude relation of a nonlinear normal mode (NNM) of a mechanical system is tracked by computing the *backbone curves* (see, e.g., [18–24]). For instance, in past years, the principle of similarity [25] has been used to suppress undesirable nonlinearities [26] and for tuning the design of nonlinear vibration absorbers [27].

This variety of applications has been supported by the development of analytical and computational tools that enable the analysis of nonlinear systems. Due to the growing complexity of the applications, these tools are often limited by the number of unknowns they can handle, which has led to further developments in the field of Reduced Order Models (ROM) [28–32]. Despite all these developments, tailoring the nonlinear dynamic response of a system remains a challenging task. The difficulty lies in finding the optimal set of system parameters such that the nonlinear response exhibits desired frequencies at specific amplitudes (see, e.g., [33]).

To overcome this limitation, optimization strategies have been laid down in the past. In [34], the *equivalent static loads method* [35,36] is used to minimize deformations and stress in large deformation problems. In this approach, the time response of the nonlinear system is evaluated. Then, for each time step, the equivalent static load is computed as the load that produces the same response as the nonlinear analysis. Therefore, in the optimization algorithm, the full nonlinear time response can be replaced by the set of linear static responses, thus simplifying the sensitivity analysis. However, the static approximation may not be able to represent important dynamic phenomena such as resonance and damping effects. In addition, the approach is not able to capture the nonlinear frequency-amplitude relation.

For applications where sensitivities are expensive or cumbersome to evaluate, *Genetic algorithms* have been found to be beneficial [37,38]. These methods work by iteratively evolving a population of candidate solutions through selection, recombination, and mutation. However, the cost of multiple nonlinear solutions over the population of each generation could lead to prohibitive computational times.

Optimization of nonlinear dynamic problems using ROMs has also been explored in some works. For example, an optimal design strategy using (damped) nonlinear normal modes (dNNMs) in combination with the extended energy balance method was presented in [39]. Here, a surrogate Kringing model is constructed from a number of full simulations for different parameter instances. This surrogate model is then used to obtain an input–output function for the computation of dNNMs and their sensitivities at unseen parameter configurations.

Dou et al. [40–42], indirectly optimized the backbone curve of geometrically nonlinear beam structures using a ROM based on normal forms [43]. Specifically, in [40] the authors developed explicit expressions for an objective function that characterizes the hardening behavior in terms of the cubic coefficient of the ROM. Computing analytic sensitivities using the adjoint method, they were able to maximize/minimize the hardening behavior of a single mode resonator, and to maximize the 2:1 modal interaction between two modes of a T-shaped beam structure. To the best of the authors' knowledge, this is the only example of analytic backbone optimization currently available in the literature, and motivates the present work. While the method described in [40] may offer valuable solutions for specific structural problems, its applicability in broader contexts may be limited by the choice of the objective function. For instance, the approach may not be suitable when the nonlinear behavior cannot be fully represented by a single ROM coefficient. On the other hand, in [41,42], the authors used a numerical opti-

mization procedure to maximize/minimize the hardening/softening behavior of the system. At each iteration, the Harmonic Balance method (HBM) [44,45] is used to compute NNMs, and sensitivities are obtained with the adjoint method to update the design variables. Employing the HBM, this method has the merit of being able to treat a larger class of nonlinearities as compared to the analytical approach in [40]. At the same time, some inherent drawbacks of the numerical method will also be present, especially regarding the HBM sensitivities [46], as multiple directions can be taken to Taylor expand the solution. This choice may ill-condition the sensitivity computation, with unpredictable outcomes, affecting the optimization results.

To summarize, all the currently available strategies to optimize the nonlinear dynamic response of a mechanical system rely either on nonlinear time simulations or the harmonic balance method, with or without reduced order models. These approaches frequently leverage indirect indicators to gauge the system's nonlinear response. To our knowledge, there are no methods that use ROMs to directly optimize the backbone curves of a nonlinear system.

To this end, the choice of a suitable ROM and the solution method is particularly critical in an optimization process. Indeed, as the references [41,42,47] also pointed out, the system can differ significantly from one optimization iteration to another. This means not only that the ROM would need to be constructed repeatedly, but also that its accuracy can vary and that the solver settings would generally require readjustments. Consider, for instance, a projection-based reduction method (e.g., implicit condensation and expansion [48–50], modal derivatives [51–54]). To retain a constant level of accuracy throughout the optimization, such a ROM would generally require a change in the size of the reduction basis. On the other hand, the choice of a reduction basis depends on the problem and often requires user input that may be difficult to automate. The backbone or the forced response is then computed using the ROM. Usually, this is achieved via numerical continuation using the collocation method (see, e.g., [55]), the harmonic balance method (see, e.g., [45]), or the shooting method (see, e.g, [56]). However, the effectiveness and accuracy of these numerical methods often rely on a set of parameters chosen by the user, such as the number of harmonics in the HBM, or the arc-length parameter for numerical continuation. These settings are typically tailored to the specific application under study. During the optimization iterations, the system's behavior might shift in unpredictable ways, thus requiring adjustments to these parameters. This issue poses a challenge in automating the procedure. Although we cannot exclude that such an approach can be successively pursued [47], we deem highly desirable an optimization procedure that is as independent as possible from user inputs.

In the present work, we develop a method to optimize the conservative backbone curves of a nonlinear mechanical system using the reduced dynamics on Lyapunov subcenter manifolds (LSM). To this end, we exploit the recent developments that enable the computation of such invariant manifolds in high-dimensional mechanical systems. These methods have been successfully applied in the calculation of forced-response in systems near resonance, [24,32], internal resonances [57,58], in the study of constrained mechanical systems [59].

Our choice of LSM-based ROMs for the optimization of backbone curves is motivated by the following considerations:

1. For generic design configurations without internal resonances, LSMs provide ROMs that are consistently two-dimensional, which leads to efficient optimization.
2. An analytic expression for the conservative backbone curve is available [24], stemming from the reduced dynamics of the LSM in polar coordinates. This avoids any numerical continuation to compute the backbone.
3. Optimization sensitivities can be computed analytically, as we will demonstrate. This results in fast convergence using gradient-based optimization techniques.
4. a computationally inexpensive a posteriori error estimate;
5. LSM can be approximated up to arbitrarily orders of accuracy in an automated fashion for any parameter configurations.

The paper is organized as follows. In Sect. 2, we recall the generic description of the nonlinear mechanical system used in this work, along with the main quantities that are used in the remainder of the paper. In Sect. 3, Lyapunov subcenter manifolds are briefly discussed, introducing the notation and the analytic expression of the backbone curve. In Sect. 4, the optimization problem is set and the optimization routine is defined, while analytic sensitivities are discussed in

Sect. 5. Finally, numerical results are shown in Sect. 6 for a spring-mass chain system with nonlinear springs and for a FE discretized von Kármán clamp-clamp beam. Conclusions are then drawn in Sect. 7.

2 Mechanical system

Consider the following equation of motion for a generic autonomous, undamped, nonlinear mechanical system:

$$\boldsymbol{M}\ddot{\boldsymbol{x}} + \boldsymbol{K}\boldsymbol{x} + \boldsymbol{f}(\boldsymbol{x}) = \boldsymbol{0}, \tag{1}$$

where $\boldsymbol{x} \in \mathbb{R}^n$ is the displacement vector, $\boldsymbol{M}$ and $\boldsymbol{K}$ are the mass and linear stiffness matrices, respectively, and $\boldsymbol{f}(\boldsymbol{x})$ is a displacement-dependent nonlinear term.

The linear normal modes are obtained by solving the generalized eigenvalue problem

$$\boldsymbol{K}\boldsymbol{\phi}_i = \omega_i^2 \boldsymbol{M}\boldsymbol{\phi}_i, \tag{2}$$

where ω_i is the i-th eigenfrequency and $\boldsymbol{\phi}_i$ is the associated mode shape vector. The mass normalization is applied, yielding

$$\boldsymbol{\phi}_i^T \boldsymbol{M}\boldsymbol{\phi}_i = 1 \quad \text{and} \quad \boldsymbol{\phi}_i^T \boldsymbol{K}\boldsymbol{\phi}_i = \omega_i^2. \tag{3}$$

In state space form, the system can be rewritten as a N-dimensional system ($N = 2n$) as

$$\boldsymbol{B}\dot{\boldsymbol{z}} = \boldsymbol{A}\boldsymbol{z} + \boldsymbol{F}(\boldsymbol{z}), \tag{4}$$

being

$$\boldsymbol{z} = \begin{bmatrix} \boldsymbol{x} \\ \dot{\boldsymbol{x}} \end{bmatrix}, \quad \boldsymbol{F}(\boldsymbol{z}) = \begin{bmatrix} \boldsymbol{0} \\ -\boldsymbol{f}(\boldsymbol{x}) \end{bmatrix}, \tag{5}$$

$$\boldsymbol{A} = \begin{bmatrix} \boldsymbol{0} & -\boldsymbol{K} \\ -\boldsymbol{K} & \boldsymbol{0} \end{bmatrix}, \quad \boldsymbol{B} = \begin{bmatrix} -\boldsymbol{K} & \boldsymbol{0} \\ \boldsymbol{0} & \boldsymbol{M} \end{bmatrix}. \tag{6}$$

For this system, the eigenvalues λ, the right eigenvectors $\boldsymbol{v}$, and the left eigenvectors $\boldsymbol{u}$ write:

$$\lambda_{2i-1} = j\omega_i \qquad \& \quad \lambda_{2i} = -j\omega_i, \tag{7a}$$

$$\boldsymbol{v}_{2i-1} = \begin{bmatrix} \boldsymbol{\phi}_i \\ j\omega_i\boldsymbol{\phi}_i \end{bmatrix} \quad \& \quad \boldsymbol{v}_{2i} = \begin{bmatrix} \boldsymbol{\phi}_i \\ -j\omega_i\boldsymbol{\phi}_i \end{bmatrix}, \tag{7b}$$

$$\boldsymbol{u}_{2i-1} = \tau_i \bar{\boldsymbol{v}}_{2i-1} \qquad \& \quad \boldsymbol{u}_{2i} = \tau_i \bar{\boldsymbol{v}}_{2i}, \tag{7c}$$

where $\bar{(\bullet)}$ denotes the complex conjugate operator, and the constant $\tau_i = -\frac{1}{2\omega_i^2}$ is used to scale the left eigenvectors in order to meet the normalization condition:

$$\boldsymbol{u}_i^* \boldsymbol{B}\boldsymbol{v}_j = \delta_{ij}, \tag{8}$$

where $(\cdot)^*$ denotes the transpose conjugate operator, and δ_{ij} is the Kronecker delta function.

The nonlinear term $\boldsymbol{F}(\boldsymbol{z})$ can be rearranged as

$$\boldsymbol{F}(\boldsymbol{z}) = \sum_{i \in \mathbb{N}} \boldsymbol{F}_i \boldsymbol{z}^{\otimes i}, \tag{9}$$

where $\boldsymbol{F}_i \in \mathbb{R}^{N \times N^i}$ is a matrix containing the coefficients of the system nonlinearity, and where $\boldsymbol{z}^{\otimes i} = \boldsymbol{z} \otimes \boldsymbol{z} \otimes \ldots \otimes \boldsymbol{z}$ (i-times), with $\otimes$ denoting the Kronecker product. Notice that Eq. (9) describes exactly only polynomial nonlinearities (such as the ones stemming from large geometric deformations in finite element models); for other types of nonlinearities, a polynomial form can still be retrieved either by recasting [60] or by using a Taylor expansion approximation.

3 LSM computation

Lyapunov subcenter manifolds are nonlinear continuations of two-dimensional modal subspaces associated with nonresonant vibration modes in conservative, unforced mechanical systems [19,23]. The reduced dynamics of an LSM consists of the nonlinear (amplitude-dependent) periodic solutions associated with the undamped free vibrations along the corresponding vibration mode. In this section, we briefly recall how to obtain LSMs (see, e.g., [23,24]), and how to analytically extract conservative backbone curves.

We denote by $\mathcal{W}(E)$ the two-dimensional LSM constructed around the master modal subspace E of system (1).

Let $\boldsymbol{W} : \mathbb{C}^2 \to \mathbb{R}^N$ be a parametrization of the 2-dimensional LSM $\mathcal{W}(E)$ and let $\boldsymbol{p} \in \mathbb{C}^2$ denote the parametrization coordinates. Furthermore, Let $\boldsymbol{R} : \mathbb{C}^2 \to \mathbb{C}^2$ be a parametrization of the reduced dynamics, such that

$$\dot{\boldsymbol{p}} = \boldsymbol{R}(\boldsymbol{p}). \tag{10}$$

Then, for any full system trajectory $\boldsymbol{z}(t)$ on $\mathcal{W}(E)$, we have a reduced dynamics trajectory $\boldsymbol{p}(t)$ such that

$$\boldsymbol{z}(t) = \boldsymbol{W}(\boldsymbol{p}(t)). \tag{11}$$

Differentiating Eq. (11) and substituting Eq. (10) into Eq. (4), we obtain the *invariance equation*

$$\boldsymbol{B}\frac{\partial \boldsymbol{W}}{\partial \boldsymbol{p}}\boldsymbol{R} = \boldsymbol{A}\boldsymbol{W} + \boldsymbol{F} \circ \boldsymbol{W}. \tag{12}$$

To compute the LSM and its reduced dynamics, we need to solve Eq. (12) for the parametrizations $\boldsymbol{W}$ and $\boldsymbol{R}$. Following [24], we expand these parametrizations in Taylor series as

$$\boldsymbol{W} = \sum_{i\in\mathbb{N}} \boldsymbol{W}_i \boldsymbol{p}^{\otimes i}, \tag{13}$$

$$\boldsymbol{R} = \sum_{i\in\mathbb{N}} \boldsymbol{R}_i \boldsymbol{p}^{\otimes i}, \tag{14}$$

where $\boldsymbol{W}_i \in \mathbb{C}^{N\times 2^i}$ and $\boldsymbol{R}_i \in \mathbb{C}^{2\times 2^i}$ are coefficient matrices to be determined.

Substituting the expansions (13) and (14) into the invariance Eq. (12), and collecting coefficients of order i, we obtain a linear system in terms of the unknowns $\boldsymbol{W}_i$, $\boldsymbol{R}_i$. At a given order i, the invariance equation depends only on quantities at orders less than or equal to i. Hence, the invariance Eq. (12) can be solved recursively up to any arbitrary order. In practice, these linear equations are vectorized in the so-called *cohomological equation*:

$$\mathcal{L}_i \mathrm{vec}(\boldsymbol{W}_i) = \boldsymbol{h}_i(\boldsymbol{R}_i), \tag{15}$$

where $\mathcal{L}_i$ is the order–i cohomological operator, and the RHS $\boldsymbol{h}_i$ is vector depending on the parametrization coefficients in $\boldsymbol{R}_i$. The latter can be computed by selecting a parametrization style. Here, we adopt the normal form style of parametrization as it allows us to analytically extract the backbone curve (see, e.g., [24]). A cubic order approximation of LSMs and their reduced dynamics in a normal form style can also be performed non-intrusively for systems with up to cubic nonlinearities following the stiffness evaluation procedure (STEP) [61], similarly to [62]. For the sake of completeness, the expressions of the terms appearing in Eq. (15) and details about its solution are synthetically reported in Appendix A.

3.1 Analytical backbone

After solving the invariance equation as described in Sect. 3, the LSM is computed using only the master mode $\boldsymbol{\phi}_m$ associated to the two-dimensional modal subspace $E = \mathrm{span}(\boldsymbol{v}_{2m-1}, \boldsymbol{v}_{2m})$. From the LSM then, the conservative backbone curve can be analytically determined (see, e.g., [63]).

If the coordinates $\boldsymbol{p}$ associated with the master mode are chosen in polar form, that is

$$\boldsymbol{p}(t) = \rho(t)\begin{bmatrix} e^{j\theta(t)} \\ e^{-j\theta(t)} \end{bmatrix}, \tag{16}$$

it can be shown that the following frequency–amplitude ($\dot{\theta} - \rho$) relationship holds [24]

$$\dot{\theta} = \omega(\rho) = \omega_m + \sum_{i\in\mathbb{N},\, i\geq 2} \gamma_i \rho^{i-1}, \tag{17}$$

where γ_i are coefficients obtained from $\boldsymbol{R}_i$. For the sake of completeness, Eq. (17) is derived in Appendix B. Finally, this expression can be evaluated for a range of polar amplitudes ρ. For each (ω, ρ) pair we can then compute the corresponding $\boldsymbol{p}(t)$ over a range $\theta(t) \in [0, 2\pi]$ and, using Eq. (11), the periodic orbit associated to each point on the backbone curve can be retrieved in physical coordinates $\boldsymbol{z}(t)$ using the LSM parametrization according to Eq. (11).

4 Backbone optimization

4.1 Problem definition

In the previous section, we have briefly recalled the steps to obtain the backbone curve of a mechanical system using the LSM reduction. Now, we want to lay down an optimization procedure to tailor the shape of such a backbone curve, by defining a discrete number of amplitude-frequency points. While selecting the target frequency is straightforward, for the "amplitude" several options are available. An easy choice would be to select directly a target ρ in the reduced dynamics, but this would be of little use for practical cases, where we want to impose a physical amplitude. In this sense, any (combination of) dof out of $\boldsymbol{z}$ may serve as a good candidate to define such an amplitude. Moreover, the "amplitude" of the periodic response associated to a

point $(\dot{\theta}, \rho)$ on the backbone, computed through Eqs. (11) and (17), is not well defined *per se*: it could be the maximum value, the amplitude of a spectral component, or a Root Mean Squared (RMS) value. In the present work, we opt for this latter choice, considering the response of a single dof of interest, identified by the extraction vector $\boldsymbol{a} \in \mathbb{N}^N$ as $z = \boldsymbol{a}^T \boldsymbol{z}$. That said, in general, the optimization problem will take the form

$$\begin{aligned} &\min_{\boldsymbol{\mu}} \ J \\ &\text{s.t.} \quad \dot{\theta}(\rho(Z_j^\star)) - \Omega_j^\star = 0, \quad \forall j \\ &\qquad \boldsymbol{\mu}_L \leq \boldsymbol{\mu} \leq \boldsymbol{\mu}_U \end{aligned} \tag{18}$$

being J the objective function, $\Omega_j^\star$ the j-th target[1] frequency associated with the target RMS amplitude $Z_j^\star$, $\boldsymbol{\mu}$ the parameter vector with upper and lower bounds ($\boldsymbol{\mu}_{U/L}$). Notice that the equality in Eq. (18) can be changed into an inequality without loss of generality. In the following, we explicitly derive an expression for $Z(\rho)$, which will be used to solve Eq. (18) and, later, to compute sensitivities.

4.2 Target amplitudes

Let us write an expression for the RMS value of the dof of interest at a given point (ω, ρ). For convenience, let us rewrite $\boldsymbol{p}$ as

$$\boldsymbol{p} = \rho \begin{bmatrix} e^{j\theta} \\ e^{-j\theta} \end{bmatrix} = \rho \tilde{\boldsymbol{p}}(\theta), \tag{19}$$

so that

$$z(\theta, \rho) = \boldsymbol{a}^T \sum_{i \in \mathbb{N}} \rho^i \boldsymbol{W}_i \tilde{\boldsymbol{p}}^{\otimes i}. \tag{20}$$

For a given system, this value is a function of ρ (constant) and θ, which tracks the evolution of reduced dynamics in time. To remove the dependence on the variable θ (and thus on time), we define a set of θ_k as

$$\theta_k \in [0, 2\pi], \quad \forall k = 1, \ldots, N_\theta \tag{21}$$

and, for each θ_k, let us we define

$$z_k(\rho) = \sum_{i \in \mathbb{N}} \rho^i \boldsymbol{a}^T \boldsymbol{W}_i \tilde{\boldsymbol{p}}_k^{\otimes i}, \tag{22}$$

where

$$\tilde{\boldsymbol{p}}_k = \begin{bmatrix} e^{j\theta_k} \\ e^{-j\theta_k} \end{bmatrix}. \tag{23}$$

Notice that the obtained set of z_k corresponds to a time discretization of the response at the given point (ω, ρ), with N_θ samples. This way, the RMS value writes

$$Z(\rho) = \sqrt{\frac{1}{N_\theta} \sum_{k=1}^{N_\theta} z_k^2(\rho)}. \tag{24}$$

Using this equation, given a target RMS value $Z^\star$, we can find the value of $\rho^\star$ (unknown) by solving $Z(\rho^\star) = Z^\star$. The resulting $\rho^\star$ can be used in Eq. (17) to find the corresponding frequency $\dot{\theta}$ and solve the optimization problem defined in (18).

In some cases, Eq. (24) might be too difficult to be solved. To get a first approximation of its solution, we can consider only the leading order ($i = 1$), thus neglecting all the higher orders. With this approximation, an explicit expression for ρ function of Z is obtained:

$$Z \approx \rho \sqrt{\frac{1}{N_\theta} \sum_{k=1}^{N_\theta} (\boldsymbol{a}^T \boldsymbol{W}_1 \tilde{\boldsymbol{p}}_k)^2}. \tag{25}$$

Equation (25) can provide a good approximate solution to be used as a starting point to initialize the numerical method used to solve Eq. (24).

4.3 Accuracy check

On top of all the optimization-related problems, in our case, we also have to take care that the LSM-based reduced order model accuracy remains consistent throughout the optimization process. Indeed, it is not guaranteed that the selected expansion order at iteration "i" will provide the same accuracy for a new parameter vector $\boldsymbol{\mu}$ at iteration "i+1". The risk, of course, is that the optimization output will be completely inaccurate (even when successful). The problem can be tackled mainly in two ways, either by selecting a fixed expansion order and performing a final a posteriori assessment of the optimization output (eventually repeating

[1] We denote target quantities with $(\bullet)^\star$.

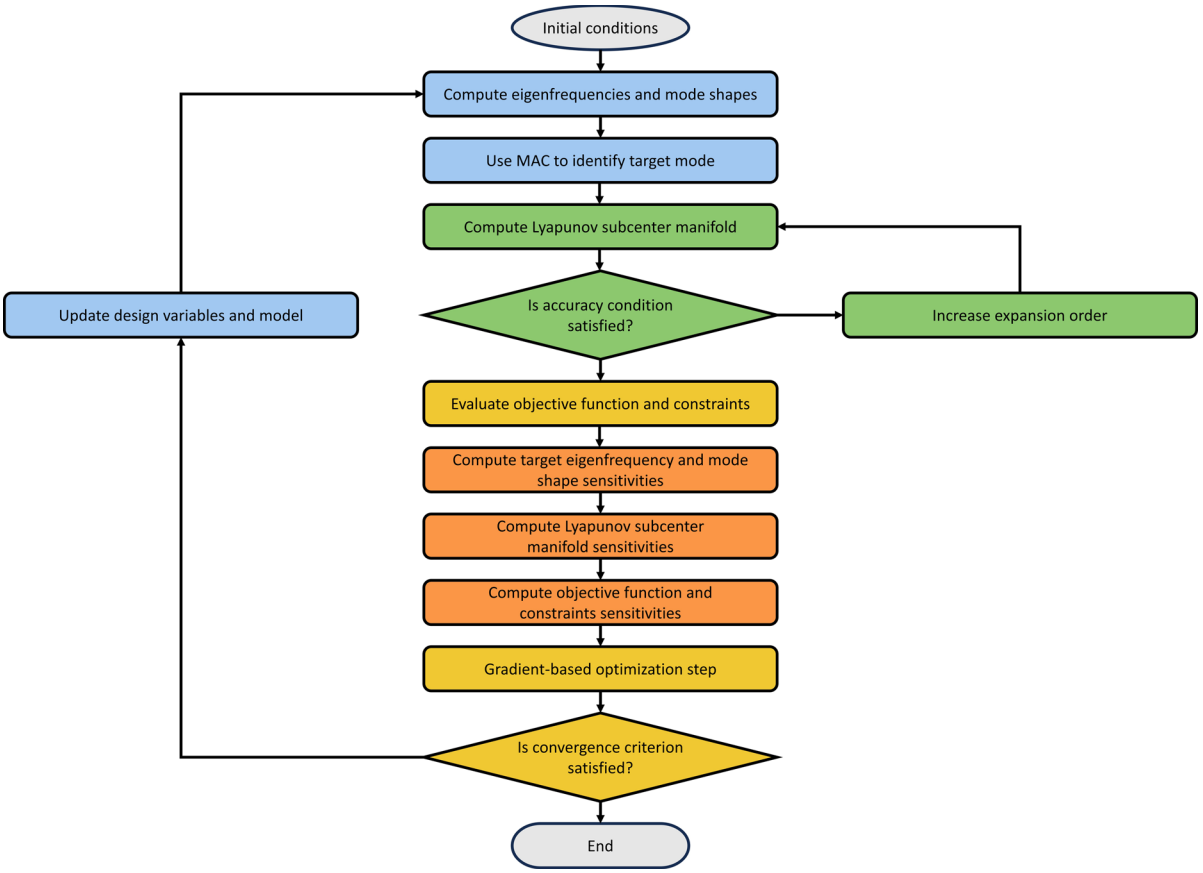

Fig. 1 Block scheme for the optimization process. The blocks relative to the system model are in blue, whereas the LSM blocks are shown in green. The yellow blocks are the ones related to the optimization problem. The sensitivity analysis, represented by the orange blocks, are computed as explained in Sect. 5. If finite differences are used instead, the orange blocks are removed and the LSM will be evaluated several times within the optimization iterations to approximate sensitivities

the optimization with a higher LSM order if the assessment fails), or by estimating the approximation error *during* the optimization, so to increase the expansion order if error tolerances are exceeded. In both cases, an error estimate is required.

Similarly to [59], we define the residual of the invariance Eq. (12) as

$$\boldsymbol{\mathcal{E}}(\boldsymbol{p}(\rho,\theta)) = \boldsymbol{B}\frac{\partial \boldsymbol{W}}{\partial \boldsymbol{p}}\boldsymbol{R} - \boldsymbol{A}\boldsymbol{W} - \boldsymbol{F}\circ\boldsymbol{W}. \tag{26}$$

A common choice is then to take the norm of the residual as an error measurement, eventually normalized over a reference quantity. In our case, we use as an error indicator the following normalized residual norm, averaged over a span $\theta_k \in [0,\ 2\pi]$ for $k = 1, \ldots, N_\theta$ (as previously done for Eq. (24)):

$$\varepsilon = \frac{1}{N_\theta}\sum_{k=1}^{N_\theta}\frac{||\boldsymbol{\mathcal{E}}(\rho_{max},\theta_k)||_2}{\Delta(\rho_{max},\theta_k)}, \tag{27}$$

where $\rho_{max} \geq \rho^\star$ is the chosen maximum amplitude to test, and

$$\Delta(\rho,\theta) = \max\left(||\boldsymbol{B}\partial_{\boldsymbol{p}}\boldsymbol{W}\boldsymbol{R}||_2,\ ||\boldsymbol{A}\boldsymbol{W}||_2,\ ||\boldsymbol{F}\circ\boldsymbol{W}||_2\right).$$

Finally, defining a tolerance ε_{tol} and checking whether $\varepsilon < \varepsilon_{tol}$, algorithms can be defined to increase the LSM expansion order (or even to lower it). Notice that the a posteriori error in Eq. (27) is computationally inexpensive to evaluate once the manifold and the parametriza-

tion are known and, therefore, it can be included in the optimization procedure without introducing a significant computational burden.

4.4 Mode–veering check

As recalled in Sect. 3, the LSM used to compute the backbone curve is defined for a master modal subspace E, spanned by the two eigenvectors of the first-order system (Eq. (4)) associated to the linear normal mode $\boldsymbol{\phi}_m$. During optimization, however, it may happen that lower and higher frequency eigenmodes switch places [64]. This means that if m is kept constant, we may end up tracking a different mode shape from the initial one. The usual way to cope with mode veering is to keep track of the objective mode m by using the Modal Assurance Criterion (MAC, [65]), which measures the similarity of mode shapes as:

$$\mathrm{MAC}_{ij} = \frac{|\boldsymbol{\phi}_i^T \boldsymbol{\phi}_j|^2}{(\boldsymbol{\phi}_i^T \boldsymbol{\phi}_i)(\boldsymbol{\phi}_j^T \boldsymbol{\phi}_j)}. \tag{28}$$

Computing the MAC between a set of modes around the m-th mode at the current iteration and $\boldsymbol{\phi}_m$ at the previous one, it is possible to change m accordingly.

4.5 Optimization routine

In conclusion, the optimization procedure presented in this section is sketched in Fig. 1, and it allows us to tailor the backbone curve of a mechanical system by defining a discrete set of target points $(\Omega^\star,\ Z^\star)$, while keeping track of the approximation error of the LSM-based reduced order model and of the target mode to be optimized. Such a scheme can be readily implemented in available optimization algorithms (e.g. *fmincon* function in Matlab) using finite differences to compute gradients. However, given the analyticity of the LSM, in the next section, we provide explicit expressions for the sensitivities.

5 Sensitivity analysis

Now, we let the mechanical system depend on some parameters, collected in the vector $\boldsymbol{\mu}$. For instance, in a nonlinear spring-mass chain, the parameters can be chosen as the physical properties of the chain, such as masses and springs. On the other hand, in the field of topology optimization of finite element models, the parameters are related to the particular method used to discretize the design domain [66–68]. To apply a gradient-based optimization algorithm, the sensitivities of the backbone curve with respect to the design variables μ are required. The derivatives of the matrices and vectors $\boldsymbol{K}$, $\boldsymbol{M}$, $\boldsymbol{f}$, $\boldsymbol{A}$, $\boldsymbol{B}$, and $\boldsymbol{F}$ depend on the formulation of the mechanical system under consideration, and are usually straightforward to compute. On the other hand, the derivative of the conservative backbone curve requires a more complex procedure that involves both the cohomological equation defined in Eq. (15) and the normal form parametrization.

Let us now consider the optimization problem defined in Eq. (18). Neglecting the sensitivities of J and of the lower/upper bounds on $\boldsymbol{\mu}$ (trivial), we have to take the derivative of the (j-th) constraint

$$\dot{\theta}(\rho(Z^\star)) - \Omega^\star \lessgtr 0, \tag{29}$$

that can be computed from Eq. (17) as

$$\begin{aligned}\frac{\mathrm{d}\dot{\theta}}{\mathrm{d}\mu} = \frac{\mathrm{d}\omega_m}{\mathrm{d}\mu} + \sum_{i=2} \frac{\mathrm{d}\gamma_i}{\mathrm{d}\mu}\rho^{i-1} \\ + \sum_{i=2} \frac{\mathrm{d}\rho}{\mathrm{d}\mu}\gamma_i(i-1)\rho^{i-2}.\end{aligned} \tag{30}$$

The sensitivity for γ_i can be obtained as

$$\frac{\mathrm{d}\gamma_i}{\mathrm{d}\mu} = \frac{1}{2}\begin{bmatrix} -j & j \end{bmatrix} \frac{\mathrm{d}\boldsymbol{R}_i}{\mathrm{d}\mu}\mathbf{1}_{2^i}. \tag{31}$$

where $\mathbf{1}_{2^i} \in \mathbb{R}^{2^i \times 1}$ is a column vector of all ones (see Appendix B).

The derivative of ω_m is computed (along with the derivative of the linear normal mode $\boldsymbol{\varphi}_m$) following standard procedures used in the optimization and sensitivity analysis of (linear) dynamical problems. Details are provided in Appendix C.

The sensitivity of ρ, instead, can be computed from the definition of the target amplitude $Z(\rho)$ in Eq. (24). Derivations are provided in Appendix D.

Notice that the aforementioned sensitivities depend on the sensitivities of the LSM with respect to the parameter μ, i.e., $\frac{\mathrm{d}\boldsymbol{W}_i}{\mathrm{d}\mu}$ and $\frac{\mathrm{d}\boldsymbol{R}_i}{\mathrm{d}\mu}$. In particular, the sensitivity of $\boldsymbol{W}_i$ is computed taking the derivative of the cohomological equation as

Algorithm 1 Sensitivity computation

1: Evaluate ρ solving Eq. (24).
2: Compute sensitivities of ω_m and ϕ_m (Eq. (C18)).
3: Compute sensitivities of $\boldsymbol{R}_1$ and $\boldsymbol{W}_1$ using Eqs. (E.28) and (E.29).
4: **while** $i \leq$ max order **do**
5: Compute sensitivities of $\boldsymbol{R}_i$ using Eq. (E.31).
6: Compute sensitivities of $\boldsymbol{W}_i$ using Eq. (32).
7: **end while**
8: Evaluate sensitivity of ρ using Eq. (D25).
9: Evaluate sensitivity of $\dot{\theta}$ using Eq. (30).

$$\mathcal{L}_i \frac{\mathrm{d}\mathrm{vec}(\boldsymbol{W}_i)}{\mathrm{d}\mu} = \frac{\mathrm{d}\boldsymbol{h}_i}{\mathrm{d}\mu} - \frac{\mathrm{d}\mathcal{L}_i}{\mathrm{d}\mu}\mathrm{vec}(\boldsymbol{W}_i), \tag{32}$$

and the sensitivity of $\boldsymbol{R}_i$ depends on the choice of parametrization style (normal form in this work). We provide the explicit expressions of the LSM sensitivities in Appendix E and discuss the solution of the under-determined system (32) in Appendix F. Algorithm 1 summarizes the steps we follow for sensitivity computation.

Remark (computational complexity). With the proposed sensitivity formulation, the computational complexity of one iteration of the optimization has an upper bound of $N_\mu\, \mathcal{O}_{\mathrm{LSM}}$, where N_μ is the number of design variables, and $\mathcal{O}_{\mathrm{LSM}}$ is the computational complexity associated to the computation of the LSM. This limit gives an indication about the maximum number of design variables that can be used in the optimization problem.

6 Numerical examples

In this section, we present some numerical examples where the optimization is carried out in Matlab, using the in-built function *fmincon* and a dedicated code implementing the computation of the LSM and its derivatives, as described in the previous sections. The optimization routine is the one described in Fig. 1.

6.1 Uniform spring-mass chain

We first consider a uniform spring-mass chain, as shown in Fig. 2. We consider the system parameters as the mass m, the linear spring constant k, and the cubic spring constant k_3, i.e., we have 3 design variables. We apply fixed boundary conditions to both ends of the chain. In this example, we use a chain made of 5 masses, and we observe the response of the middle mass at the 1st eigenfrequency.

Table 1 Initial values, lower bounds, and upper bounds of the design variables for the examples in Sects. 6.1 and 6.2

Design variable		Initial value	Lower bound	Upper bound
m	[kg]	3.0	1.0	10.0
k	[N/m]	30.0	10.0	50.0
k_2	[N/m^2]	3.0	0.1	5.0
k_3	[N/m^3]	3.0	0.1	5.0

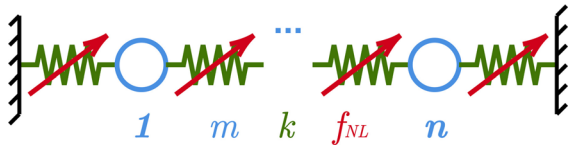

Fig. 2 Scheme of a spring mass chain with uniform properties. Fixed boundary conditions are applied to both ends of the chain. In a chain with n masses m, there are $n+1$ connections, each one characterized by linear stiffness k and nonlinear force $f_{NL} = k_3 \Delta x^3$

The optimization problem is stated as:

$$\begin{aligned} &\min_{\boldsymbol{\mu}} \; k_3 \\ &\text{s.t.} \quad \dot{\theta}(\rho(Z_j^\star)) - \Omega_j^\star = 0, \quad \forall j = 1, 2 \\ &\qquad \boldsymbol{\mu}_L \leq \boldsymbol{\mu} \leq \boldsymbol{\mu}_U \end{aligned} \tag{33}$$

where the objective function aims at minimizing the nonlinear term (cubic spring). The initial conditions and the limits on the design variables are specified in Table 1, whereas the target points are

$$(\Omega_1^\star, Z_1^\star) = (2.0, 0.0),$$
$$(\Omega_2^\star, Z_2^\star) = (2.1, 2.0).$$

Throughout the optimization process, a constant LSM expansion of order 7 is considered. The solution is shown in Fig. 3. The backbone of the optimal solution in Fig. 3 is validated using time simulations, with forward- and backward-going stepped-sines at different forcing levels. To avoid numerical singularities during the integration, a damping ratio $\xi = 0.05$ is used. A damper of value $c = 2m\omega_0\xi$ is then added in parallel to each springs. Figure 4 shows the results of the numerical simulations, along with the conservative backbone,

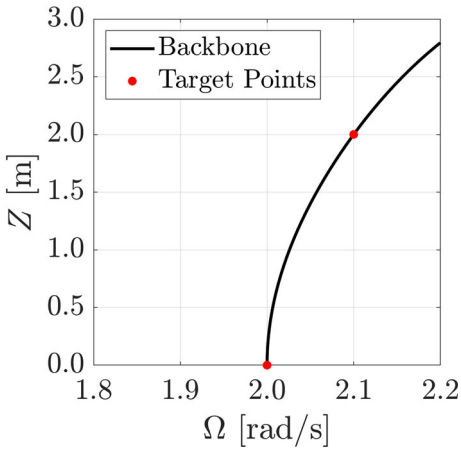

Fig. 3 Optimal solution obtained by solving (33) with $(\Omega_1^\star, Z_1^\star) = (2.0, 0.0)$ and $(\Omega_2^\star, Z_2^\star) = (2.1, 2.0)$. The optimization converges to a solution with $m = 1$, $k = 14.93$, and $k_3 = 1.34$

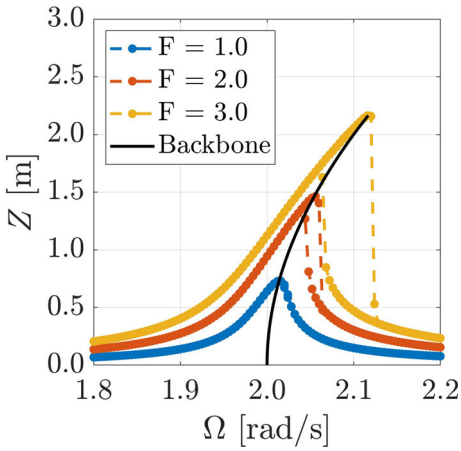

Fig. 4 Numerical results of the optimal solution in Fig. 3 obtained through frequency sweeps at different forcing levels. The numerical results are compared to the backbone

showing good agreement. Notice, however, that validation of the LSM reduction method results has been extensively discussed in other contributions [24], and it will not be addressed anymore in the present work.

Remark (feasibility). Not all optimization problems have a feasible solution. This is the case when the target points are not physically admissible by the system, in general, or at least within the parameter boundaries.

For instance, the uniform spring-mass chain presented in this section, having only positive cubic springs, cannot exhibit a softening behavior. Indeed,

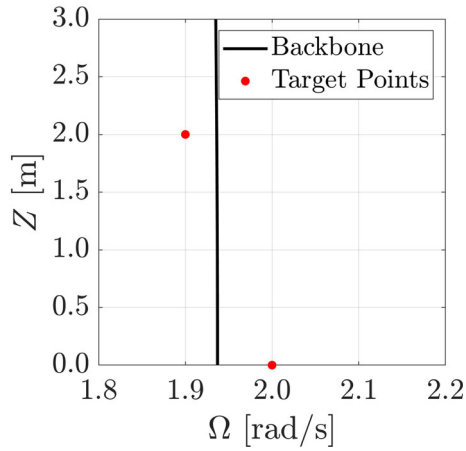

Fig. 5 Backbone for the uniform spring-mass chain system, computed at the last converged iteration of the optimization problem defined in Eq. (33). Before failing, the optimization stops at a solution with $m = 3.58$, $k = 50.12$, and $k_3 = -0.04$

trying to solve Eq. (33) with target points

$$(\Omega_1^\star, Z_1^\star) = (2.0, 0.0),$$
$$(\Omega_2^\star, Z_2^\star) = (1.9, 2.0),$$

that define a nonlinear behavior of the softening type, results in an unfeasible solution, reported in Fig. 5 for completeness.

6.2 Non-uniform spring-mass chain

In this section, we consider a nonuniform spring-mass chain with linear, quadratic, and cubic springs (Fig. 6), where all the mass and linear, quadratic and cubic stiffness values are treated as independent design variables (namely, m_i, k_i, $k_{2,i}$, $k_{3,i}$, with i denoting the mass ordinal). Again, fixed boundary conditions are applied to both ends of the chain.

In this example, we use a chain made of 3 masses, and we focus on the response of the middle mass at the 1st eigenfrequency. The optimization problem is stated as:

$$\begin{aligned} &\min_{\boldsymbol{\mu}} \ \textstyle\sum_{i=1}^{3} m_i \\ &\text{s.t.} \quad \dot{\theta}(\rho(Z_1^\star)) - \Omega_1^\star = 0 \\ &\qquad \dot{\theta}(\rho(Z_2^\star)) - \Omega_2^\star \le 0 \\ &\qquad \dot{\theta}(\rho(Z_3^\star)) - \Omega_3^\star \ge 0 \\ &\qquad \boldsymbol{\mu}_L \le \boldsymbol{\mu} \le \boldsymbol{\mu}_U \end{aligned} \tag{34}$$

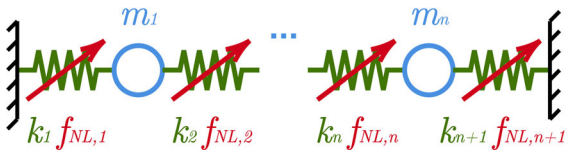

Fig. 6 Scheme of a spring mass chain with non uniform properties. Fixed boundary conditions are applied to both ends of the chain. In a chain with n different masses m_i, there are $n+1$ connections, each one characterized by different linear stiffness k_i and nonlinear force $f_{NL,i} = k_{2,i}(x_i - x_{i-1})^2 + k_{3,i}(x_i - x_{i-1})^3$

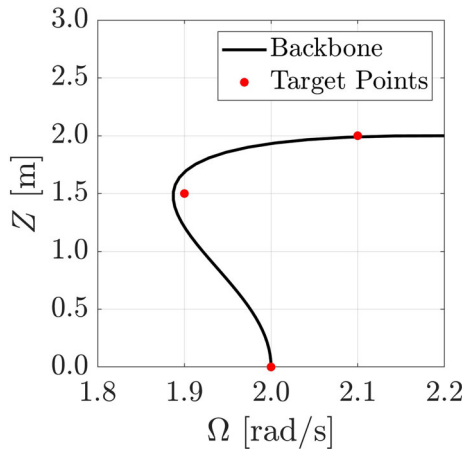

Fig. 7 Backbone curve corresponding to the optimal solution, obtained by solving the problem defined in Eq. (34). The optimization converges to the solution reported in Table 2

where the objective function aims at minimizing the total mass of the system in order to obtain a lightweight chain. The initial conditions and the limits on the design variables are again the ones specified in Table 1 (the limits are the same $\forall i$), while the target points are

$$(\Omega_1^\star, Z_1^\star) = (2.0, 0.0),$$
$$(\Omega_2^\star, Z_2^\star) = (1.9, 1.5),$$
$$(\Omega_3^\star, Z_3^\star) = (2.1, 2.0),$$

and describe a softening/hardening behavior of the system. Again, a constant LSM expansion of order 7 is considered. The optimal solution is shown in Fig. 7 and in Table 2. As it can be seen from this result, as opposed to the one presented in Fig. 5, the more freedom is given to the optimization problem in terms of design variables and in terms of the "complexity" of the nonlinear forces (that here include also quadratic terms), the higher is the degree with which we can shape the backbone of the system.

Table 2 Optimal solution for the 15 design variables of the non-uniform spring-mass chain system, obtained by solving the problem defined in Eq. (34)

Design variable		Optimal values			
		$i=1$	$i=2$	$i=3$	$i=4$
m_i	[kg]	4.427	1.000	4.161	–
k_i	[N/m]	39.17	21.54	11.81	12.35
$k_{2,i}$	[N/m^2]	1.307	1.476	3.109	4.531
$k_{3,i}$	[N/m^3]	4.098	3.507	2.498	0.347

6.3 A von Kármán beam

In this last example, we present the case of a geometrically nonlinear, clamp-clamp von Kármán beam. The structure is described by a finite element model consisting of 10 von Kármán elements (27 degrees of freedom). As design variables, we take the beam thickness h, the length L, and the amplitudes A_1 and A_2 which define the shape of the beam as

$$y = A_1 \sin(\pi x/L) + A_2 \sin(2\pi x/L),$$

being $x \in \{0, L\}$ and y the nodal coordinates of the beam. The material is characterized by Young's modulus equal to 90 GPa, Poisson's ratio of 0.3, and density corresponding to 7850 kg/m^3. Given the complexity of the problem, the derivatives of matrices $\boldsymbol{A}$, $\boldsymbol{B}$ and $\boldsymbol{F}_i$ with respect to the parameters (necessary to compute the sensitivities) are hereby computed numerically using finite differences. The computations have been carried out in YetAnotherFEcode (v1.3.0) [69], an open source FE code for Matlab. Initial values and bounds for the design variables are reported in Table 3. The optimization problem is stated as follows:

$$\begin{aligned} &\min_{\boldsymbol{\mu}} \; A_2 L \\ &\text{s.t.} \quad \dot{\theta}\left(\rho\left(\tfrac{1}{5}h_0\right)\right) - \omega_0 = 0 \\ &\qquad \dot{\theta}\left(\rho\left(\tfrac{2}{5}h_0\right)\right) - 0.95\,\omega_0 = 0 \\ &\qquad \boldsymbol{\mu}_L \le \boldsymbol{\mu} \le \boldsymbol{\mu}_U \end{aligned} \tag{35}$$

where h_0 is the initial thickness, and ω_0 is the first eigenfrequency of the system (evaluated using the initial parameters). During the optimization procedure,

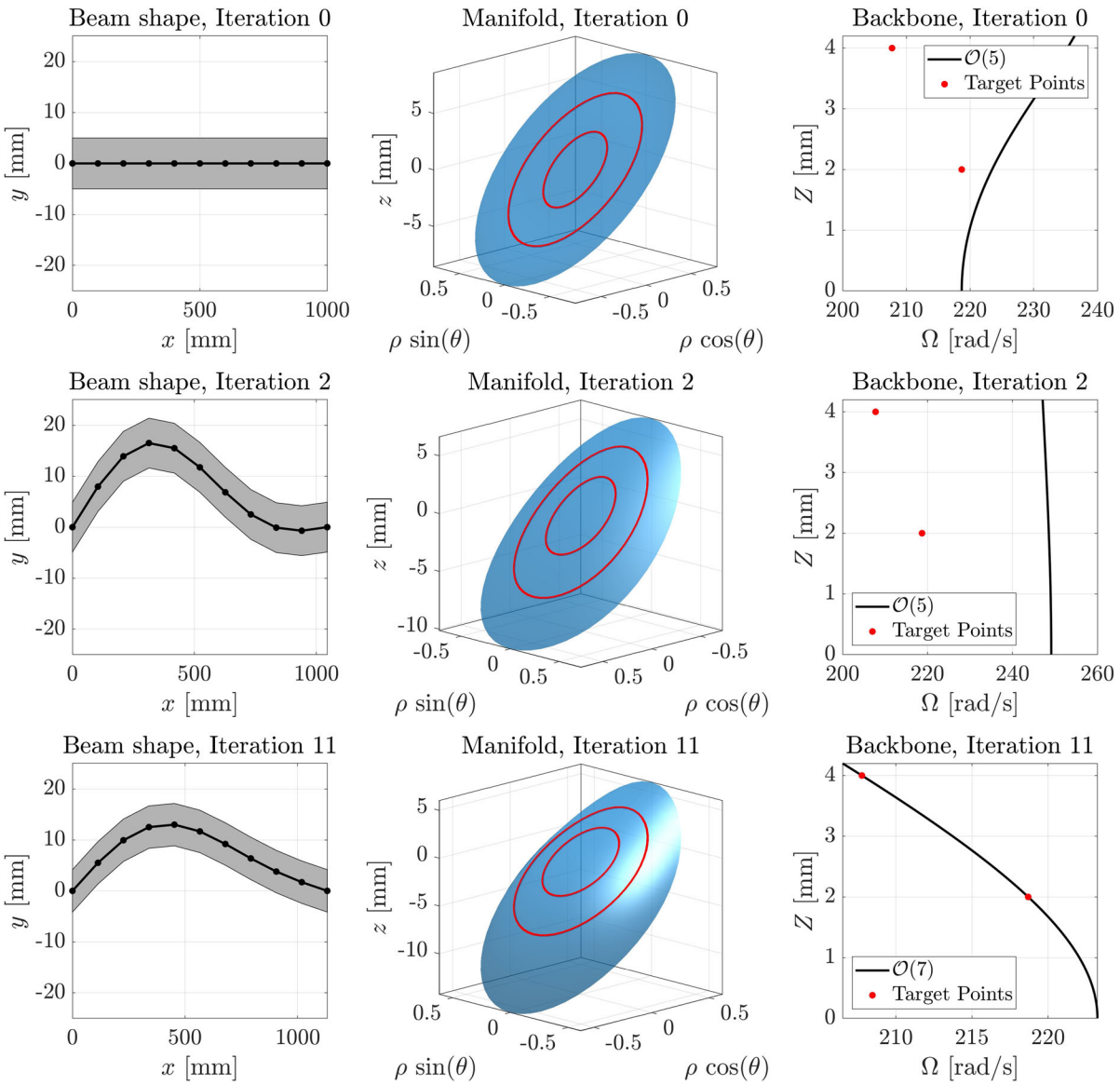

Fig. 8 Snapshots of three optimization iterations for a finite element model of a clamp-clamp beam, discretized with 10 von Kármán beam finite elements. The design variables are the beam thickness h, length L, and the amplitude A_1 and A_2 of two sinusoidal shapes. Left column: beam geometry (notice that the beam thickness is uniform, although it appears distorted due to the different scaling of the two axes). Central column: manifold (light blue surface) and orbits associated with the target points (red lines). Right column: backbone curves (black lines), and target points (red dots)

mode–veering and error checks have been enabled, so that the first mode is always tracked and so that, when the error measure ε (Eq. (27)) exceeds a threshold value ε_{tol}, the LSM expansion order is increased at the next iteration. This threshold is empirically selected upon a convergence study of the LSM on the system, using the initial design parameters.

The frequency constraints have been satisfied in 5 iterations, whereas the convergence has been reached in 11 iterations. Figure 8 shows the snapshots of three iterations of the optimization, showing the evolution of

Table 3 Initial values, lower bounds, and upper bounds of the design variables for the von Kármán beam example

Design variable		Initial value	Lower bound	Upper bound
A_1	[mm]	0	0	20
A_2	[mm]	0	0	20
h	[mm]	10	1	100
L	[mm]	1000	500	1500

the geometry (left column), the manifold (middle column), and the backbone curve (right column). Notice that the expansion order has been increased from 5 to 7 in order to satisfy the accuracy condition (Eq. (27)). Comparing the final solution using an LSM of orders 7 and 11, only a minor deviation is observed, indicating order 7 to be sufficient for this example. The comparison is shown in Fig. 9.

For the sake of completeness, we report that the overall computational time was about 4.8 min on a Windows laptop equipped with Intel Core i7-1255U CPU @ 1.70 GHz and 16.0 GB RAM. The peak memory consumption during the optimization was around 2 GB, mainly associated with the LSM computation. This relatively high cost is mainly to be imputed to a sub-optimal code implementation, which can certainly be improved, for instance, by integrating the sensitivity routines in the SSMTool [70], which is specialized for Spectral Submanifold (SSM) calculation. Nonetheless, the use of the LSM and the analytical expressions for sensitivity computations make the proposed approach efficient compared to traditional methods that rely on expensive full-system simulations and numerical continuation.

Finally, we remark once more on the importance of both selecting feasible targets (i.e., allowed by the physics) and using a suitable set of parameters. For instance, in this example, if only the A_1 parameter was retained and a softening behavior (of the like of problem (35)) was targeted, the optimization would fail. Indeed, increasing A_1 would create an arc shape, which on the one hand leads to a softening behavior, but on the other hand also increases the linear natural frequency of the system, so that the target points cannot be reached. This limit can be overcome by letting the thickness and/or the length vary. However, as in many gradient-based optimization problems, there is no general rule for selecting the proper design parameters and initial conditions. Moreover, the number and type of design

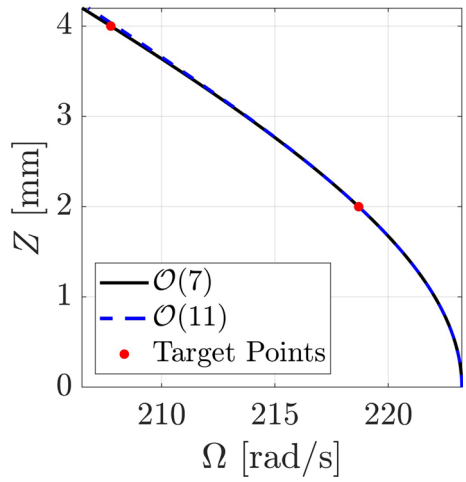

Fig. 9 Backbone of the von Kármán beam example, computed for the optimal solution of problem (35). Order 7 (black, solid line) and order 11 (blue, dashed) solutions show only a minor discrepancy at high amplitude

variables usually depend on the specific application, and they cannot be chosen by the user. For instance, in many practical examples, the lower and upper bounds are related to the characteristics of the production process or to design limitations. The same consideration applies for the target points of the optimization problem, which are defined by the design requirements. Even so, we can conclude that, as a general rule, the more the system can "change", the more freedom we have in selecting the target points for the backbone, but this, obviously, comes at the expense of longer computational times.

7 Conclusions

In this work, we proposed a gradient-based optimization procedure for the optimization of the backbone curve of a generic mechanical system, described by a set of parameters. This is done by selecting a number of target frequency-amplitude points and exploiting the analytic expression of the backbone given by the LSM, which allowed us to directly evaluate both the backbone curve and the associated sensitivities, without any numerical solution. An error estimate has also been introduced in order to make sure that the same level of accuracy is maintained throughout the optimization process. The procedure has proved to be inherently robust, for it does not depend on user inputs, if

not for the initial expansion order of the LSM (which is automatically adjusted) and, of course, on the target points. Finally, numerical examples of two spring-mass chain systems and of a von Kármán clamp-clamp beam have been provided, and the feasibility of the optimization targets has been discussed. Although currently restricted to a limited number of design variables, we think that the proposed strategy can be adapted to topology optimization, e.g. by means of the adjoint method to compute the sensitivities. Moreover, using LSMs and the same LSM sensitivities provided in this work, more applications can be envisioned, such as the optimization of forced-frequency responses, multiple modes with internal resonances, and parametric amplification.

Acknowledgements The authors acknowledge the financial support of STMicroelectronics.

Author contributions M.P. and J.M. conceptualized the work and wrote the main manuscript text. The main code was written by M.P., aided by J.M.. S.J. supervised and contributed to theoretical developments. F.B. supervised the work. All the authors reviewed the manuscript.

Funding Open access funding provided by Politecnico di Milano within the CRUI-CARE Agreement. STMicroelectronics (award number 4000614871).

Data Availibility No datasets were generated or analysed during the current study.

Declarations

Conflict of interest On behalf of all authors, the corresponding author states that there is no Conflict of interest.

Ethical approval The manuscript does not contain clinical studies or patient data.

Informed consent Text

Replication of results The analytical expressions for the backbone and its sensitivity have been presented throughout the paper, along with all the parameters used in the optimization problems. This information should allow to comfortably replicate the results obtained using, for instance, the SSMTool [70].

Appendix A

Cohomological equation The terms appearing in the cohomological Eq. (15) are listed below:

$$\mathcal{L}_i = \mathcal{R}_{i,i}^T \otimes \boldsymbol{B} - \boldsymbol{I}_{2^i} \otimes \boldsymbol{A}, \tag{A1a}$$

$$\mathcal{R}_{i,i} = \sum_{k=1}^{i} \boldsymbol{I}_2^{\otimes k-1} \otimes \boldsymbol{R}_1 \otimes \boldsymbol{I}_2^{\otimes i-k}, \tag{A1b}$$

$$\boldsymbol{h}_i = \mathrm{vec}(\boldsymbol{C}_i) - \boldsymbol{D}_i \mathrm{vec}(\boldsymbol{R}_i), \tag{A1c}$$

$$\boldsymbol{D}_i = \boldsymbol{I}_{2^i} \otimes (\boldsymbol{B}\boldsymbol{W}_1), \tag{A1d}$$

$$\boldsymbol{C_i} = (\boldsymbol{F} \circ \boldsymbol{W})_i - \boldsymbol{B} \sum_{j=2}^{i-1} \boldsymbol{W}_j \mathcal{R}_{i,j}, \tag{A1e}$$

$$\mathcal{R}_{i,j} = \sum_{k=1}^{j} \boldsymbol{I_2}^{\otimes k-1} \otimes \boldsymbol{R}_{i-j+1} \otimes \boldsymbol{I_2}^{\otimes j-k}, \tag{A1f}$$

$$(\boldsymbol{F} \circ \boldsymbol{W})_i = \sum_{j=2}^{i} \boldsymbol{F}_j \left(\sum_{\boldsymbol{q} \in \mathbb{N}^j}^{|\boldsymbol{q}|=i} \boldsymbol{W}_{q_1} \otimes \cdots \otimes \boldsymbol{W}_{q_j} \right). \tag{A1g}$$

At each order $i \geq 2$, the cohomological Eq. (15) must be solved for the coefficients $\boldsymbol{W}_i$. However, to do so, the coefficients in $\boldsymbol{R}_i$ are required. We choose the normal-form style of parametrization of the reduced dynamics which results in coefficients $\boldsymbol{R}_i$ as (see, e.g., [24])

$$\mathrm{vec}(\boldsymbol{R}_i) = \boldsymbol{E}_i \boldsymbol{N}_i^* \mathrm{vec}(\boldsymbol{C}_i), \tag{A2}$$

being $\boldsymbol{E}_i$ and $\boldsymbol{N}_i$ matrices whose columns are of the form

$$\boldsymbol{E}_i = \left[\cdots, \boldsymbol{e}_\ell^{\boldsymbol{R}} \otimes \boldsymbol{e}_j, \cdots \right], \tag{A3a}$$

$$\boldsymbol{N}_i = \left[\cdots, \boldsymbol{e}_\ell^{\boldsymbol{R}} \otimes \boldsymbol{u}_j, \cdots \right], \tag{A3b}$$

where $\boldsymbol{e}_\ell^{\boldsymbol{R}}$ and $\boldsymbol{e}_j$ are the basis vectors of properly selected spaces, and where the pair (ℓ, j) denotes an

Table 4 Dimensions of relevant matrices and vectors involved in the LSM computation

Name	Dimensions
$\boldsymbol{F}_i$	$\in \mathbb{C}^{N\times N^i}$
$\boldsymbol{W}_i$	$\in \mathbb{C}^{N\times 2^i}$
$\boldsymbol{R}_i$	$\in \mathbb{C}^{2\times 2^i}$
$\mathcal{L}_i$	$\in \mathbb{C}^{N\cdot 2^i\times N\cdot 2^i}$
$\boldsymbol{h}_i$	$\in \mathbb{C}^{N\cdot 2^i}$
$\boldsymbol{D}_i$	$\in \mathbb{C}^{N\cdot 2^i\times 2^{i+1}}$
$\boldsymbol{C}_i$	$\in \mathbb{C}^{N\times 2^i}$
$(\boldsymbol{F}\circ\boldsymbol{W})_i$	$\in \mathbb{C}^{N\times 2^i}$
$\mathcal{R}_{i,j}$	$\in \mathbb{C}^{2^j\times 2^i}$
$\boldsymbol{E}_i\boldsymbol{N}_i^*$	$\in \mathbb{C}^{2\cdot 2^i\times N\cdot 2^i}$

inner resonance. Notice that Eq. (A2) can be directly evaluated once the lower orders are known.

To initialize the computation, a sensible choice is to set at the leading order ($i = 1$)

$$\boldsymbol{R}_1 = \boldsymbol{\Lambda}_E, \tag{A4a}$$
$$\boldsymbol{W}_1 = \boldsymbol{V}_E, \tag{A4b}$$

where, for the master space E, we defined

$$\boldsymbol{\Lambda}_E = \begin{bmatrix} j\omega_m & 0 \\ 0 & -j\omega_m \end{bmatrix}, \tag{A5a}$$
$$\boldsymbol{V}_E = \begin{bmatrix} \boldsymbol{\phi}_m & \boldsymbol{\phi}_m \\ j\omega_m\boldsymbol{\phi}_m & -j\omega_m\boldsymbol{\phi}_m \end{bmatrix}, \tag{A5b}$$
$$\boldsymbol{U}_E = \tau \begin{bmatrix} \boldsymbol{\phi}_m & \boldsymbol{\phi}_m \\ -j\omega_m\boldsymbol{\phi}_m & j\omega_m\boldsymbol{\phi}_m \end{bmatrix}, \tag{A5c}$$

with the normalization factor $\tau = -1/(2\omega_m^2)$.

Table 4 summarizes the dimensions of the matrices and vectors involved in the cohomological equation.

Appendix B

On the backbone curve coefficients

Differentiating Eq. (16), we get

$$\dot{\boldsymbol{p}} = \dot{\rho}\begin{bmatrix} e^{j\theta} \\ e^{-j\theta} \end{bmatrix} + \rho\dot{\theta}\begin{bmatrix} je^{j\theta} \\ -je^{-j\theta} \end{bmatrix}, \tag{B6}$$

which, by definition (10), is also equal to

$$\dot{\boldsymbol{p}} = \sum_{i\in\mathbb{N}} \boldsymbol{R}_i\rho^i \begin{bmatrix} e^{j\theta} \\ e^{-j\theta} \end{bmatrix}^{\otimes i}. \tag{B7}$$

Due to the inner resonances, matrix $\boldsymbol{R}_i$ takes on a particular structure, and it can be shown that the only surviving exponential terms in the above equation are the ones in $\pm jk\theta$ with $k = 1$, while all terms with $k \neq 1$ multiply null entries of $\boldsymbol{R}_i$. Also, noticing that all the terms in $e^{j\theta}$ and $e^{-j\theta}$ sum up on the first and second rows, respectively, after some manipulation, we can rewrite Eq. (B7) as:

$$\dot{\boldsymbol{p}} = \sum_{i\in\mathbb{N}} \rho^i \begin{bmatrix} e^{j\theta} & 0 \\ 0 & e^{-j\theta} \end{bmatrix} \boldsymbol{r}_i, \tag{B8}$$

where

$$\boldsymbol{r}_i = \boldsymbol{R}_i\mathbf{1}_{2^i} \in \mathbb{R}^{2\times 1}, \tag{B9}$$

being $\mathbf{1}_{2^i} \in \mathbb{R}^{2^i\times 1}$ a column vector of all ones.

Equaling Eqs. (B6) and (B8) and simplifying the exponential, we get:

$$\begin{cases} \dot{\rho} = \frac{1}{2}\sum_{i\in\mathbb{N}} \rho^i \left(r_{i,1} + r_{i,2}\right) \\ \dot{\theta} = -j\frac{1}{2}\sum_{i\in\mathbb{N}} \rho^{i-1}\left(r_{i,1} - r_{i,2}\right) \end{cases} \tag{B10}$$

We now take a generic order i, and rewrite the coefficients $r_{i,1}$ and $r_{i,2}$ as

$$\begin{aligned} r_{i,1} &= \beta_{i,1} + j\gamma_{i,1}, \\ r_{i,2} &= \beta_{i,2} + j\gamma_{i,2}. \end{aligned} \tag{B11}$$

We know that both ρ and θ are real quantities, and we need both $\dot{\rho}$ and $\dot{\theta}$ to be real as well. Thus, we can write the following conditions:

$$\begin{aligned} \Im(r_{i,1} + r_{i,2}) = 0 \;&\rightarrow\; \gamma_{i,2} = -\gamma_{i,1} \\ \Im(-jr_{i,1} + jr_{i,2}) = 0 \;&\rightarrow\; \beta_{i,2} = \beta_{i,1} \end{aligned} \tag{B12}$$

This means that $r_{i,1}$ and $r_{i,2}$ are complex conjugate. Moreover, since we are considering steady state, we have $\dot{\rho} = 0$, so it follows that

$$\Re(r_{i,1} + r_{i,2}) = 0 \rightarrow \beta_{i,2} = \beta_{i,1} = 0 \tag{B13}$$

Therefore, we can simplify the notation as

$$r_{i,1} = \bar{r}_{i,2} = j\gamma_i \tag{B14}$$

In the end, considering that at leading order we have $\gamma_1 = \omega_m$, the conservative backbone in Eq. (17) is retrieved using:

$$\gamma_i = \frac{1}{2}\left[-j \;\; j\right] \boldsymbol{R}_i \mathbf{1}_{2^i}. \tag{B15}$$

Appendix C

Eigenfrequency sensitivity

The sensitivity analysis involves the derivative of the master mode shape $\boldsymbol{\phi}_m$ and its relative eigenfrequency ω_m [71,72]. To compute them, we start differentiating Eq. (2):

$$\begin{aligned} -2\omega_m \frac{\mathrm{d}\omega_m}{\mathrm{d}\mu}\boldsymbol{M}\boldsymbol{\phi}_m + \left(-\omega_m^2 \frac{\mathrm{d}\boldsymbol{M}}{\mathrm{d}\mu} + \frac{\mathrm{d}\boldsymbol{K}}{\mathrm{d}\mu}\right)\boldsymbol{\phi}_m \\ + \left(-\omega_m^2 \boldsymbol{M} + \boldsymbol{K}\right)\frac{\mathrm{d}\boldsymbol{\phi}_m}{\mathrm{d}\mu} = \mathbf{0}. \end{aligned} \tag{C16}$$

The mass normalization condition (Eq. (3)) is derived as well, yielding

$$2\boldsymbol{\phi}_m^T \boldsymbol{M} \frac{\mathrm{d}\boldsymbol{\phi}_m}{\mathrm{d}\mu} + \boldsymbol{\phi}_m^T \frac{\mathrm{d}\boldsymbol{M}}{\mathrm{d}\mu}\boldsymbol{\phi}_m = 0. \tag{C17}$$

Equations (C16) and (C17) are combined in a linear system whose unknowns are the derivatives of mode shape and eigenfrequency:

$$\begin{aligned} \begin{bmatrix} -\omega_m^2 \boldsymbol{M} + \boldsymbol{K} & -2\omega_m \boldsymbol{M}\boldsymbol{\phi}_m \\ -2\omega_m \boldsymbol{\phi}_m^T \boldsymbol{M} & 0 \end{bmatrix} \begin{bmatrix} \frac{\mathrm{d}\boldsymbol{\phi}_m}{\mathrm{d}\mu} \\ \frac{\mathrm{d}\omega_m}{\mathrm{d}\mu} \end{bmatrix} = \\ \begin{bmatrix} \left(-\omega_m^2 \frac{\mathrm{d}\boldsymbol{M}}{\mathrm{d}\mu} + \frac{\mathrm{d}\boldsymbol{K}}{\mathrm{d}\mu}\right)\boldsymbol{\phi}_m \\ \omega_m \boldsymbol{\phi}_m^T \frac{\mathrm{d}\boldsymbol{M}}{\mathrm{d}\mu}\boldsymbol{\phi}_m \end{bmatrix}. \end{aligned} \tag{C18}$$

Equation (C18) must be solved for each design variable, making the overall computational cost proportional to the size of the optimization problem. In case of a large number of design variables, for instance as in topology optimization, this formulation would not be feasible, and an alternative approach should be used. Nonetheless, Eq. (C18) can still be used in many practical problems where a parametric optimization approach can be used with a limited set of design variables.

Appendix D

Sensitivity of ρ

The value of ρ in Eq. (30) depends on the physical amplitude that we are considering. As discussed in Sect. 4.2, ρ is defined setting a target $Z^\star$ by[2]

$$Z^\star = \sqrt{\frac{1}{N_\theta}\sum_k z_k^2}, \tag{D19}$$

that can be rewritten as

$$\underbrace{N_\theta \left(Z^\star\right)^2}_{\text{constant}} = \sum_k z_k^2 = Y, \tag{D20}$$

with

$$z_k = \sum_i \rho^i \boldsymbol{a}^T \boldsymbol{W}_i \tilde{\boldsymbol{p}}_k^{\otimes i} = \sum_i \rho^i c_{i,k}. \tag{D21}$$

Taking the absolute variation of Eq. (D20) with respect to μ, we have

$$0 = \frac{\mathrm{d}Y}{\mathrm{d}\mu} = \frac{\partial Y}{\partial \mu} + \frac{\partial Y}{\partial \rho}\frac{\mathrm{d}\rho}{\mathrm{d}\mu}, \tag{D22}$$

where

$$\frac{\partial Y}{\partial \mu} = \sum_k \frac{\partial Y}{\partial z_k}\frac{\partial z_k}{\partial \mu} = 2\sum_k \sum_i z_k \rho^i \frac{\partial c_{i,k}}{\partial \mu}, \tag{D23a}$$

$$\frac{\partial Y}{\partial \rho} = \sum_k \frac{\partial Y}{\partial z_k}\frac{\partial z_k}{\partial \rho} = 2\sum_k \sum_i z_k i \rho^{i-1} c_{i,k}, \tag{D23b}$$

and

$$\frac{\partial c_{i,k}}{\partial \mu} = \boldsymbol{a}^T \frac{\partial \boldsymbol{W}_i}{\partial \mu}\tilde{\boldsymbol{p}_k}^{\otimes i}. \tag{D24}$$

Finally, solving Eq. (D22), the sensitivity for ρ reads:

$$\frac{\mathrm{d}\rho}{\mathrm{d}\mu} = -\frac{\sum_k \sum_i z_k \rho^i \boldsymbol{a}^T \frac{\partial \boldsymbol{W}_i}{\partial \mu}\tilde{\boldsymbol{p}_k}^{\otimes i}}{\sum_k \sum_i z_k i \rho^{i-1} \boldsymbol{a}^T \boldsymbol{W}_i \tilde{\boldsymbol{p}}_k^{\otimes i}}. \tag{D25}$$

[2] To ease the reading, in the sums that follow we indicate only the indexes, whose ranges are implicitly assumed.

Appendix E

Lyapunov subcenter manifold sensitivities

As mentioned in Sect. 5, all the sensitivities ultimately depend on how the manifold and its parametrization change with the design parameters. In this section, we thus turn our attention to the sensitivities of the LSM.

E.1 Preliminary considerations

Before deep diving into the derivatives, let us reformulate some terms in a convenient form for the discussion that will follow. Considering Eq. (A5), we can write:

$$\boldsymbol{\Lambda}_E = \omega_m \begin{bmatrix} j & 0 \\ 0 & -j \end{bmatrix} = \omega_m \tilde{\boldsymbol{\Lambda}}_E, \tag{E.26a}$$

$$\boldsymbol{V}_E = \begin{bmatrix} 1 & 1 \\ j\omega_m & -j\omega_m \end{bmatrix} \otimes \boldsymbol{\phi}_m = \tilde{\boldsymbol{V}}_E \otimes \boldsymbol{\phi}_m, \tag{E.26b}$$

$$\boldsymbol{U}_E = \tau \begin{bmatrix} 1 & 1 \\ -j\omega_m & j\omega_m \end{bmatrix} \otimes \boldsymbol{\phi}_m = \tilde{\boldsymbol{U}}_E \otimes \boldsymbol{\phi}_m. \tag{E.26c}$$

Similarly, we can rewrite Eq. (A3b) as

$$\begin{aligned} \boldsymbol{N}_i &= \left[\cdots, \boldsymbol{e}_\ell^{\boldsymbol{R}} \otimes \boldsymbol{u}_j, \cdots \right] \\ &= \left[\cdots, \boldsymbol{e}_\ell^{\boldsymbol{R}} \otimes \tilde{\boldsymbol{u}}_j \otimes \boldsymbol{\phi}_m, \cdots \right] \\ &= \left[\cdots, \boldsymbol{e}_\ell^{\boldsymbol{R}} \otimes \tilde{\boldsymbol{u}}_j, \cdots \right] \otimes \boldsymbol{\phi}_m \\ &= \left[\cdots, \boldsymbol{e}_\ell^{\boldsymbol{R}} \otimes \left(\tilde{\boldsymbol{U}}_E \boldsymbol{e}_j \right), \cdots \right] \otimes \boldsymbol{\phi}_m \\ &= \tilde{\boldsymbol{N}}_i \otimes \boldsymbol{\phi}_m. \end{aligned} \tag{E.27}$$

E.2 Leading order terms

First of all, using Eq. (A4a) and (E.26a), we can compute the derivative of $\boldsymbol{R}_1$ simply as

$$\frac{\mathrm{d}\boldsymbol{R}_1}{\mathrm{d}\mu} = \frac{\mathrm{d}\omega_m}{\mathrm{d}\mu} \tilde{\boldsymbol{\Lambda}}_E, \tag{E.28}$$

where the derivative of ω_m was obtained from Eq. (C18).

In a similar way, using Eqs. (A4b) and (E.26b), we take the derivative according to the chain rule:

$$\frac{\mathrm{d}\boldsymbol{W}_1}{\mathrm{d}\mu} = \frac{\partial \tilde{\boldsymbol{V}}_E}{\partial \omega_m} \frac{\partial \omega_m}{\partial \mu} \otimes \boldsymbol{\phi}_m + \tilde{\boldsymbol{V}}_E \otimes \frac{\mathrm{d}\boldsymbol{\phi}_m}{\mathrm{d}\mu}, \tag{E.29}$$

where the derivative of $\boldsymbol{\phi}_m$ was obtained from Eq. (C18), and where

$$\frac{\partial \tilde{\boldsymbol{V}}_E}{\partial \omega_m} = \begin{bmatrix} 0 & 0 \\ j & -j \end{bmatrix}. \tag{E.30}$$

E.3 Higher order terms

Consider the matrix $\boldsymbol{R}_i$. This comes from the normal form parametrization (Eq. (A2)) that involves the matrices $\boldsymbol{E}_i$, $\boldsymbol{N}_i$, and $\boldsymbol{C}_i$. The derivative of $\boldsymbol{R}_i$ is written as

$$\begin{aligned} \frac{\mathrm{dvec}(\boldsymbol{R}_i)}{\mathrm{d}\mu} &= \boldsymbol{E}_i \frac{\mathrm{d}\boldsymbol{N}_i^*}{\mathrm{d}\mu} \mathrm{vec}(\boldsymbol{C}_i) \\ &\quad + \boldsymbol{E}_i \boldsymbol{N}_i^* \frac{\mathrm{dvec}(\boldsymbol{C}_i)}{\mathrm{d}\mu}, \end{aligned} \tag{E.31}$$

where $\boldsymbol{E}_i$ is a constant boolean matrix defined in Eq. (A3a).

The chain rule can be applied to find the derivative of matrix $\boldsymbol{N}_i$:

$$\frac{\mathrm{d}\boldsymbol{N}_i}{\mathrm{d}\mu} = \frac{\partial \tilde{\boldsymbol{N}}_i}{\partial \omega_m} \frac{\partial \omega_m}{\partial \mu} \otimes \boldsymbol{\phi}_m + \tilde{\boldsymbol{N}}_i \otimes \frac{\mathrm{d}\boldsymbol{\phi}_m}{\mathrm{d}\mu}. \tag{E.32}$$

where

$$\frac{\partial \tilde{\boldsymbol{N}}_i}{\partial \omega_m} = \left[\cdots, \boldsymbol{e}_\ell^{\boldsymbol{R}} \otimes \left(\frac{\partial \tilde{\boldsymbol{U}}_E}{\partial \omega_m} \boldsymbol{e}_j \right), \cdots \right], \tag{E.33}$$

and

$$\frac{\partial \tilde{\boldsymbol{U}}_E}{\partial \omega_m} = \frac{1}{2\omega_m^3} \begin{bmatrix} 2 & 2 \\ -j\omega_m & j\omega_m \end{bmatrix}. \tag{E.34}$$

We now focus on the derivation of matrix $\boldsymbol{C}_i$:

$$\begin{aligned} \frac{\mathrm{d}\boldsymbol{C}_i}{\mathrm{d}\mu} &= \frac{\mathrm{d}}{\mathrm{d}\mu} \left[(\boldsymbol{F} \circ \boldsymbol{W})_i \right] - \frac{\mathrm{d}\boldsymbol{B}}{\mathrm{d}\mu} \sum_{j=2}^{i-1} \boldsymbol{W}_j \boldsymbol{\mathcal{R}}_{i,j} \\ &\quad - \boldsymbol{B} \sum_{j=2}^{i-1} \frac{\mathrm{d}\boldsymbol{W}_j}{\mathrm{d}\mu} \boldsymbol{\mathcal{R}}_{i,j} - \boldsymbol{B} \sum_{j=2}^{i-1} \boldsymbol{W}_j \frac{\mathrm{d}\boldsymbol{\mathcal{R}}_{i,j}}{\mathrm{d}\mu}, \end{aligned} \tag{E.35}$$

where

$$\frac{\mathrm{d}\mathcal{R}_{i,j}}{\mathrm{d}\mu} = \sum_{k=1}^{j} \boldsymbol{I}_2^{\otimes k-1} \otimes \frac{\mathrm{d}\boldsymbol{R}_{i-j+1}}{\mathrm{d}\mu} \otimes \boldsymbol{I}_2^{\otimes j-k}, \tag{E.36}$$

and

$$\begin{aligned}\frac{\mathrm{d}}{\mathrm{d}\mu}\left[(\boldsymbol{F}\circ\boldsymbol{W})_i\right] = \\ = \sum_{j=2}^{i} \frac{\mathrm{d}\boldsymbol{F}_j}{\mathrm{d}\mu}\left(\sum_{\boldsymbol{q}\in\mathbb{N}^j}^{|\boldsymbol{q}|=i} \boldsymbol{W}_{q_1}\otimes\cdots\otimes\boldsymbol{W}_{q_j}\right) \\ + \sum_{j=2}^{i} \boldsymbol{F}_j\left[\left(\sum_{\boldsymbol{q}\in\mathbb{N}^j}^{|\boldsymbol{q}|=i} \frac{\mathrm{d}\boldsymbol{W}_{q_1}}{\mathrm{d}\mu}\otimes\cdots\otimes\boldsymbol{W}_{q_j}\right)\right. \\ \left. + \cdots + \left(\sum_{\boldsymbol{q}\in\mathbb{N}^j}^{|\boldsymbol{q}|=i} \boldsymbol{W}_{q_1}\otimes\cdots\otimes\frac{\mathrm{d}\boldsymbol{W}_{q_j}}{\mathrm{d}\mu}\right)\right].\end{aligned} \tag{E.37}$$

The last thing that remains to be addressed is the derivative of matrix $\boldsymbol{W}_i$, which appears in several terms (Eqs. (D25), (E.35) and (E.37)). One way to do this is through the derivative of the cohomological equation (Eq. (15)), which reads:

$$\frac{\mathrm{d}\mathcal{L}_i}{\mathrm{d}\mu}\mathrm{vec}(\boldsymbol{W}_i) + \mathcal{L}_i\frac{\mathrm{dvec}(\boldsymbol{W}_i)}{\mathrm{d}\mu} = \frac{\mathrm{d}\boldsymbol{h}_i}{\mathrm{d}\mu}, \tag{E.38}$$

where

$$\begin{aligned}\frac{\mathrm{d}\mathcal{L}_i}{\mathrm{d}\mu} = \frac{\mathrm{d}\mathcal{R}_{i,i}^T}{\mathrm{d}\mu}\otimes\boldsymbol{B} \\ + \mathcal{R}_{i,i}^T\otimes\frac{\mathrm{d}\boldsymbol{B}}{\mathrm{d}\mu} - \boldsymbol{I}_{2^i}\otimes\frac{\mathrm{d}\boldsymbol{A}}{\mathrm{d}\mu},\end{aligned} \tag{E.39}$$

and, from Eqs. (A1b) and (E.28):

$$\begin{aligned}\frac{\mathrm{d}\mathcal{R}_{i,i}}{\mathrm{d}\mu} &= \sum_{k=1}^{i} \boldsymbol{I}_2^{\otimes k-1}\otimes\frac{\mathrm{d}\omega_m}{\mathrm{d}\mu}\tilde{\boldsymbol{\Lambda}}_E\otimes\boldsymbol{I}_2^{\otimes i-k} \\ &= \frac{\mathrm{d}\omega_m}{\mathrm{d}\mu}\tilde{\mathcal{R}}_{i,i}.\end{aligned} \tag{E.40}$$

The derivative of the RHS of Eq. (E.38) is computed as

$$\begin{aligned}\frac{\mathrm{d}\boldsymbol{h}_i}{\mathrm{d}\mu} = \frac{\mathrm{dvec}(\boldsymbol{C}_i)}{\mathrm{d}\mu} \\ - \frac{\mathrm{d}\boldsymbol{D}_i}{\mathrm{d}\mu}\mathrm{vec}(\boldsymbol{R}_i) - \boldsymbol{D}_i\frac{\mathrm{dvec}(\boldsymbol{R}_i)}{\mathrm{d}\mu},\end{aligned} \tag{E.41}$$

with

$$\frac{\mathrm{d}\boldsymbol{D}_i}{\mathrm{d}\mu} = \boldsymbol{I}_{2^i}\otimes\left(\frac{\mathrm{d}\boldsymbol{B}}{\mathrm{d}\mu}\boldsymbol{W}_1 + \boldsymbol{B}\frac{\mathrm{d}\boldsymbol{W}_1}{\mathrm{d}\mu}\right). \tag{E.42}$$

Finally, Eq. (32) is retrieved by solving Eq. (E.38) (see also Appendix F).

Equation (32) is computationally expensive as it must be solved for each design variable. As said in Appendix C, using Eq. (32) to compute the sensitivity of $\boldsymbol{W}_i$ is an approach only suitable for parametric optimization problems with a limited set of design variables.

Appendix F

On the solution of the derivative of the cohomological equation

In the presence or in the neighborhood of inner resonances, the matrix $\mathcal{L}_i$ may become singular or ill-conditioned. This issue was discussed at length in [24], where it was shown that the parametrization (here, the normal form style) can be chosen so that the RHS of the cohomological Eq. (15) belongs to the image of the operator $\mathcal{L}_i$, allowing a solution. The derivative of the cohomological Eq. (32) also suffers from this problem, and benefits from the same solution, as proved hereafter.

Equation (32), indeed, has solutions only if its right-hand side lies in the null space of matrix $\mathcal{L}_i$. In other words, the projection of the RHS of Eq. (E.38) onto the left kernel $\mathcal{N}_i$ of matrix $\mathcal{L}_i$ must be zero.

In order to prove this, we project Eq. (15) onto $\mathcal{N}_i$ and then we differentiate it:

$$\begin{aligned}\frac{\mathrm{d}\boldsymbol{N}_i^*}{\mathrm{d}\mu}\left(\mathcal{L}_i\mathrm{vec}(\boldsymbol{W}_i)-\boldsymbol{h}_i\right)\\ +\boldsymbol{N}_i^*\left(\mathcal{L}_i\frac{\mathrm{dvec}(\boldsymbol{W}_i)}{\mathrm{d}\mu}\right.\\ \left.+\frac{\mathrm{d}\mathcal{L}_i}{\mathrm{d}\mu}\mathrm{vec}(\boldsymbol{W}_i)-\frac{\mathrm{d}\boldsymbol{h}_i}{\mathrm{d}\mu}\right)=\boldsymbol{0},\end{aligned} \tag{F43}$$

where $\boldsymbol{N}_i$ (Eq. (E.27)) is a basis for $\mathcal{N}_i$.

By definition, the projection of $\mathcal{L}_i$ onto $\mathcal{N}_i$ is identically zero, that is

$$\boldsymbol{N}_i^*\mathcal{L}_i=\boldsymbol{0}. \tag{F44}$$

Moreover, the first term in Eq. (F43) contains the cohomological equation, and therefore it is identically zero as well. Therefore, Eq. (F43) becomes:

$$\boldsymbol{N}_i^*\left(\frac{\mathrm{d}\boldsymbol{h}_i}{\mathrm{d}\mu}-\frac{\mathrm{d}\mathcal{L}_i}{\mathrm{d}\mu}\mathrm{vec}(\boldsymbol{W}_i)\right)=\boldsymbol{0}. \tag{F45}$$

This means that the right-hand side of Eq. (32) lies in the null space of matrix $\mathcal{L}_i$, thus admitting solutions.

References

1. Lifshitz, R., Cross, M.C.: Nonlinear Dynamics of Nanomechanical and Micromechanical Resonators, pp. 1–52. Wiley, London (2008)
2. Rhoads, J.F., Shaw, S.W., Turner, K.L.: Nonlinear dynamics and its applications in micro- and nanoresonators. J. Dyn. Syst. Meas. Contr. **132**(3), 034001 (2010). https://doi.org/10.1115/1.4001333
3. Zhang, W., Baskaran, R., Turner, K.L.: Effect of cubic nonlinearity on auto-parametrically amplified resonant mems mass sensor. Sens. Actuators, A **102**(1), 139–150 (2002). https://doi.org/10.1016/S0924-4247(02)00299-6
4. Meesala, V.C., Hajj, M.R., Abdel-Rahman, E.: Bifurcation-based mems mass sensors. Int. J. Mech. Sci. **180**, 105705 (2020). https://doi.org/10.1016/j.ijmecsci.2020.105705
5. Nitzan, S.H., Zega, V., Li, M., Ahn, C.H., Corigliano, A., Kenny, T.W., Horsley, D.A.: Self-induced parametric amplification arising from nonlinear elastic coupling in a micromechanical resonating disk gyroscope. Sci. Rep. **5**(1), 9036 (2015). https://doi.org/10.1038/srep09036
6. Marconi, J., Bonaccorsi, G., Giannini, D., Falorni, L., Braghin, F.: In 2021 IEEE International Symposium on Inertial Sensors and Systems (INERTIAL) (IEEE, 2021), pp. 1–4. https://doi.org/10.1109/INERTIAL51137.2021.9430478
7. Polunin, P.M., Shaw, S.W.: Maximizing the rate sensitivity of resonating gyroscopes using nonlinear shape optimization. J. Micromech. Microeng. **32**(6), 064003 (2022). https://doi.org/10.1088/1361-6439/ac6c74
8. Qalandar, K.R., Strachan, B.S., Gibson, B., Sharma, M., Ma, A., Shaw, S.W., Turner, K.L.: Frequency division using a micromechanical resonance cascade. Appl. Phys. Lett. **105**(24), 244103 (2014). https://doi.org/10.1063/1.4904465
9. Antonio, D., Zanette, D.H., López, D.: Frequency stabilization in nonlinear micromechanical oscillators. Nat. Commun. **3**(1), 806 (2012). https://doi.org/10.1038/ncomms1813
10. Villanueva, L.G., Kenig, E., Karabalin, R.B., Matheny, M.H., Lifshitz, R., Cross, M.C., Roukes, M.L.: Surpassing fundamental limits of oscillators using nonlinear resonators. Phys. Rev. Lett. **110**, 177208 (2013). https://doi.org/10.1103/PhysRevLett.110.177208
11. Hajati, A., Kim, S.G.: Ultra-wide bandwidth piezoelectric energy harvesting. Appl. Phys. Lett. **99**(8), 083105 (2011). https://doi.org/10.1063/1.3629551
12. Daqaq, M.F., Masana, R., Erturk, A., Quinn, D.: Dane: on the role of nonlinearities in vibratory energy harvesting: a critical review and discussion. Appl. Mech. Rev. **66**(4), 040801 (2014)
13. Gourdon, E., Alexander, N., Taylor, C., Lamarque, C., Pernot, S.: Nonlinear energy pumping under transient forcing with strongly nonlinear coupling: theoretical and experimental results. J. Sound Vib. **300**(3), 522–551 (2007). https://doi.org/10.1016/j.jsv.2006.06.074
14. Nucera, F., Lo Iacono, F., McFarland, D., Bergman, L., Vakakis, A.: Application of broadband nonlinear targeted energy transfers for seismic mitigation of a shear frame: Experimental results. J. Sound Vib. **313**(1), 57–76 (2008). https://doi.org/10.1016/j.jsv.2007.11.018
15. Bellet, R., Cochelin, B., Herzog, P., Mattei, P.O.: Experimental study of targeted energy transfer from an acoustic system to a nonlinear membrane absorber. J. Sound Vib. **329**(14), 2768–2791 (2010). https://doi.org/10.1016/j.jsv.2010.01.029
16. Ding, H., Chen, L.Q.: Designs, analysis, and applications of nonlinear energy sinks. Nonlinear Dyn. **100**(4), 3061–3107 (2020). https://doi.org/10.1007/s11071-020-05724-1
17. Vakakis, A.F., Gendelman, O.V., Bergman, L.A., Mojahed, A., Gzal, M.: Nonlinear targeted energy transfer: state of the art and new perspectives. Nonlinear Dyn. **108**(2), 711–741 (2022). https://doi.org/10.1007/s11071-022-07216-w
18. Rosenberg, R.M.: The normal modes of nonlinear n-degree-of-freedom systems. J. Appl. Mech. **29**, 7–14 (1962). https://doi.org/10.1115/1.3636501
19. Kelley, A.: Analytic two-dimensional subcenter manifolds for systems with an integral. Pac. J. Math. **29**, 335–350 (1969). https://doi.org/10.2140/pjm.1969.29.335
20. Kerschen, G., Peeters, M., Golinval, J.C., Vakakis, A.F.: Nonlinear normal modes, part I: a useful framework for the structural dynamicist. Mech. Syst. Signal Process. **23**(1), 170–194 (2009). https://doi.org/10.1016/j.ymssp.2008.04.002
21. Haller, G., Ponsioen, S.: Nonlinear normal modes and spectral submanifolds: existence, uniqueness and use in model reduction. Nonlinear Dyn. **86**(3), 1493–1534 (2016). https://doi.org/10.1007/s11071-016-2974-z

22. Ponsioen, S., Pedergnana, T., Haller, G.: Automated computation of autonomous spectral submanifolds for nonlinear modal analysis. J. Sound Vib. **420**, 269–295 (2018). https://doi.org/10.1016/j.jsv.2018.01.048
23. Veraszto, Z., Ponsioen, S., Haller, G.: Explicit third-order model reduction formulas for general nonlinear mechanical systems. J. Sound Vib. **468**, 115039 (2020). https://doi.org/10.1016/j.jsv.2019.115039
24. Jain, S., Haller, G.: How to compute invariant manifolds and their reduced dynamics in high-dimensional finite element models. Nonlinear Dyn. **107**(2), 1417–1450 (2022). https://doi.org/10.1007/s11071-021-06957-4
25. Habib, G., Detroux, T., Viguié, R., Kerschen, G.: Nonlinear generalization of den Hartog's equal-peak method. Mech. Syst. Signal Process. **52–53**, 17–28 (2015). https://doi.org/10.1016/j.ymssp.2014.08.009
26. Habib, G., Grappasonni, C., Kerschen, G.: Passive linearization of nonlinear resonances. J. Appl. Phys. **120**(4), 044901 (2016). https://doi.org/10.1063/1.4959814
27. Habib, G., Kerschen, G.: A principle of similarity for nonlinear vibration absorbers. Physica D **332**, 1–8 (2016). https://doi.org/10.1016/j.physd.2016.06.001
28. Mignolet, M.P., Przekop, A., Rizzi, S.A., Spottswood, S.M.: A review of indirect/non-intrusive reduced order modeling of nonlinear geometric structures. J. Sound Vib. **332**(10), 2437–2460 (2013). https://doi.org/10.1016/j.jsv.2012.10.017
29. Benner, P., Gugercin, S., Willcox, K.: A survey of projection-based model reduction methods for parametric dynamical systems. SIAM Rev. **57**(4), 483–531 (2015). https://doi.org/10.1137/130932715
30. Tiso, P., Mahdiabadi, M.K., Marconi, J.: Modal Methods for Reduced Order Modeling, pp. 97–138. De Gruyter, Berlin (2021). https://doi.org/10.1515/9783110498967-004
31. Vizzaccaro, A., Salles, L., Touzé, C.: Comparison of nonlinear mappings for reduced-order modelling of vibrating structures: normal form theory and quadratic manifold method with modal derivatives. Nonlinear Dyn. (2020). https://doi.org/10.1007/s11071-020-05813-1
32. Ponsioen, S., Jain, S., Haller, G.: Model reduction to spectral submanifolds and forced-response calculation in high-dimensional mechanical systems. J. Sound Vib. **488**, 115640 (2020). https://doi.org/10.1016/j.jsv.2020.115640
33. Detroux, T., Noël, J.P., Kerschen, G.: Tailoring the resonances of nonlinear mechanical systems. Nonlinear Dyn. **103**, 3611–3624 (2021). https://doi.org/10.1007/s11071-020-06002-w
34. Kim, Y.I., Park, G.J.: Nonlinear dynamic response structural optimization using equivalent static loads. Comput. Methods Appl. Mech. Eng. **199**(9), 660–676 (2010). https://doi.org/10.1016/j.cma.2009.10.014
35. Kang, B., Choi, W., Park, G.: Structural optimization under equivalent static loads transformed from dynamic loads based on displacement. Comput. Struct. **79**(2), 145–154 (2001). https://doi.org/10.1016/S0045-7949(00)00127-9
36. Shin, M.K., Park, K.J., Park, G.J.: Optimization of structures with nonlinear behavior using equivalent loads. Comput. Methods Appl. Mech. Eng. **196**(4), 1154–1167 (2007). https://doi.org/10.1016/j.cma.2006.09.001
37. Mollik, T., Geng, Y., Shougat, M.R.E.U., Fitzgerald, T., Perkins, E.: Genetic algorithm shape optimization to manipulate the nonlinear response of a clamped-clamped beam. Heliyon **8**(11), e11833 (2022). https://doi.org/10.1016/j.heliyon.2022.e11833
38. Denimal, E., El Haddad, F., Wong, C., Salles, L.: Topological optimization of under-platform dampers with moving morphable components and global optimization algorithm for nonlinear frequency response. J. Eng. Gas Turbines Power **143**(2), 021021 (2021). https://doi.org/10.1115/1.4049666
39. Sun, Y., Denimal, E., Yuan, J., Salles, L.: Geometric design of friction ring dampers in blisks using nonlinear modal analysis and Kriging surrogate model. Struct. Multidiscip. Optim. **65**(3), 1–25 (2022). https://doi.org/10.1007/s00158-021-03093-w
40. Dou, S., Strachan, B.S., Shaw, S.W., Jensen, J.S.: Structural optimization for nonlinear dynamic response. Philos. Trans. R. Soc. Math. Phys. Eng. Sci. **373**(2051), 20140408 (2015). https://doi.org/10.1098/rsta.2014.0408
41. Dou, S., Jensen, J.S.: Optimization of nonlinear structural resonance using the incremental harmonic balance method. J. Sound Vib. **334**, 239–254 (2015). https://doi.org/10.1016/j.jsv.2014.08.023
42. Dou, S., Jensen, J.S.: Optimization of hardening/softening behavior of plane frame structures using nonlinear normal modes. Comput. Struct. **164**, 63–74 (2016). https://doi.org/10.1016/j.compstruc.2015.11.001
43. Guckenheimer, J., Holmes, P.: Nonlinear oscillations, dynamical systems, and bifurcations of vector fields. Appl. Math. Sci. **42**, 947–947 (1986). https://doi.org/10.1007/978-1-4612-1140-2
44. Lau, S.L., Cheung, Y.K.: Amplitude incremental variational principle for nonlinear vibration of elastic systems. J. Appl. Mech. **48**, 959–964 (1981). https://doi.org/10.1115/1.3157762
45. Krack, M., Gross, J.: Harmonic Balance for Nonlinear Vibration Problems, p. 159. Mathematical Engineering Springer International Publishing, Cham (2019)
46. Saccani, A., Marconi, J., Tiso, P.: Sensitivity analysis of nonlinear frequency response of defected structures. Nonlinear Dyn. (2022). https://doi.org/10.1007/s11071-022-08064-4
47. He, X., Yang, L., Li, K., Pang, Y., Kan, Z., Song, X.: A novel geometric nonlinear reduced order modeling method using multi-fidelity surrogate for real-time structural analysis. Struct. Multidiscip. Optim. **66**(11), 1–21 (2023). https://doi.org/10.1007/s00158-023-03689-4
48. McEwan, M., Wright, J., Cooper, J., Leung, A.: A combined modal/finite element analysis technique for the dynamic response of a non-linear beam to harmonic excitation. J. Sound Vib. **243**, 601–624 (2001). https://doi.org/10.1006/jsvi.2000.3434
49. McEwan, M., Wright, J., Cooper, J., Leung, A.: In: *19th AIAA Applied Aerodynamics Conference* (American Institute of Aeronautics and Astronautics, 2001). https://doi.org/10.2514/6.2001-1595
50. Hollkamp, J.J., Gordon, R.W.: Reduced-order models for nonlinear response prediction: implicit condensation and expansion. J. Sound Vib. **318**, 1139–1153 (2008). https://doi.org/10.1016/j.jsv.2008.04.035
51. Nelson, R.B.: Simplified calculation of eigenvector derivatives. AIAA J. **14**, 1201–1205 (1976). https://doi.org/10.2514/3.7211

52. Idelsohn, S.R., Cardona, A.: A load-dependent basis for reduced nonlinear structural dynamics. Comput. Struct. **20**, 203–210 (1985). https://doi.org/10.1016/0045-7949(85)90069-0
53. Idelsohn, S.R., Cardona, A.: A reduction method for nonlinear structural dynamic analysis. Comput. Methods Appl. Mech. Eng. **49**, 253–279 (1985). https://doi.org/10.1016/0045-7825(85)90125-2
54. Slaats, P., de Jongh, J., Sauren, A.: Model reduction tools for nonlinear structural dynamics. Comput. Struct. **54**, 1155–1171 (1995). https://doi.org/10.1016/0045-7949(94)00389-K
55. Dankowicz, H., Schilder, F.: *Recipes for continuation* (Society for Industrial and Applied Mathematics, Philadelphia, PA, 2013). https://doi.org/10.1137/1.9781611972573
56. Kerschen, G., Viguié, R., Golinval, J.C., Peeters, M., Sérandour, G.: Nonlinear normal modes, part II: toward a practical computation using numerical continuation techniques. Mech. Syst. Signal Process. **23**(1), 195–216 (2008). https://doi.org/10.1016/j.ymssp.2008.04.003
57. Li, M., Jain, S., Haller, G.: Nonlinear analysis of forced mechanical systems with internal resonance using spectral submanifolds, part I: periodic response and forced response curve. Nonlinear Dyn. **110**(2), 1005–1043 (2022). https://doi.org/10.1007/s11071-022-07714-x
58. Li, M., Haller, G.: Nonlinear analysis of forced mechanical systems with internal resonance using spectral submanifolds, part II: bifurcation and quasi-periodic response. Nonlinear Dyn. **110**(2), 1045–1080 (2022). https://doi.org/10.1007/s11071-022-07476-6
59. Li, M., Jain, S., Haller, G.: Model reduction for constrained mechanical systems via spectral submanifolds. Nonlinear Dyn. **111**, 8881–8911 (2023). https://doi.org/10.1007/s11071-023-08300-5
60. Guillot, L., Cochelin, B., Vergez, C.: A generic and efficient Taylor series-based continuation method using a quadratic recast of smooth nonlinear systems. Int. J. Numer. Meth. Eng. **119**(4), 261–280 (2019). https://doi.org/10.1002/nme.6049
61. Muravyov, A.A., Rizzi, S.A.: Determination of nonlinear stiffness with application to random vibration of geometrically nonlinear structures. Comput. Struct. **81**, 1513–1523 (2003). https://doi.org/10.1016/S0045-7949(03)00145-7
62. Vizzaccaro, A., Shen, Y., Salles, L., Blahoš, J., Touzé, C.: Direct computation of nonlinear mapping via normal form for reduced-order models of finite element nonlinear structures. Comput. Methods Appl. Mech. Eng. **384**, 113957 (2021). https://doi.org/10.1016/j.cma.2021.113957
63. Breunung, T., Haller, G.: Explicit backbone curves from spectral submanifolds of forced-damped nonlinear mechanical systems. *Proceedings of the Royal Society A: Mathematical, Physical and Engineering Sciences* **474**(2213) (2018)
64. Pozzi, M., Bonaccorsi, G., Braghin, F.: A temperature-robust level-set approach for eigenfrequency optimization. Struct. Multidiscip. Optim. (2023). https://doi.org/10.1007/s00158-023-03622-9
65. Kim, T.S., Kim, Y.Y.: Mac-based mode-tracking in structural topology optimization. Comput. Struct. **74**, 375–383 (2000). https://doi.org/10.1016/S0045-7949(99)00056-5
66. Bendsøe, M.P., Sigmund, O.: Topology Optimization: Theory Methods and Applications. Springer, Berlin Heidelberg (2004)
67. Guo, X., Zhang, W., Zhong, W.: Doing topology optimization explicitly and geometrically-a new moving morphable components based framework. J. Appl. Mech. (2014). https://doi.org/10.1115/1.4027609
68. Jauregui, C.M., Hyun, J., Neofytou, A., Gray, J.S., Kim, H.A.: Avoiding reinventing the wheel: reusable open-source topology optimization software. Struct. Multidiscip. Optim. **66**, 145 (2023). https://doi.org/10.1007/s00158-023-03589-7
69. Jain, S. Marconi, J., Tiso, P.: Yetanotherfecode v1.3.0. Zenodo (2022). https://doi.org/10.5281/zenodo.7313486
70. Jain, S., Li, M., Thurnher, T., Haller, G.: SSMTool 2.5: computation of invariant manifolds in high-dimensional mechanics problems. Zenodo (2023). https://doi.org/10.5281/zenodo.10018285
71. Jain, S., Tiso, P., Rutzmoser, J.B., Rixen, D.J.: A quadratic manifold for model order reduction of nonlinear structural dynamics. Comput. Struct. **188**, 80–94 (2017). https://doi.org/10.1016/j.compstruc.2017.04.005
72. Giannini, D., Bonaccorsi, G., Braghin, F.: Size optimization of MEMS gyroscopes using substructuring. Eur. J. Mech. A/Solids (2020). https://doi.org/10.1016/j.euromechsol.2020.104045